



Received Date : 31-Dec-2018

Accepted Date : 06-Mar-2019

**Threshold Protective Effect of Deuterated Polyunsaturated Fatty Acids
on Peroxidation of Lipid Bilayers**

Alexander M. Firsov^a, Maksim A. Fomich^b, Andrei V. Bekish^b, Olga L. Sharko^b,
Elena A. Kotova^a, Harry J. Saal^c, Dragoslav Vidovic^d, Vadim V. Shmanai^b, Derek A. Pratt^e
Yuri N. Antonenko^{a*}, Mikhail S. Shchepinov^{c*}

^a*Belozersky Institute of Physico-Chemical Biology, Lomonosov Moscow State University, Moscow 119991, Russia.*

^b*Institute of Physical Organic Chemistry, National Academy of Science, Minsk 220072, Belarus.*

^c*Retrotope, Inc., Los Altos, CA 94022, USA.*

^d*Monash University, Wellington Rd, Clayton VIC 3800, Melbourne, Australia.*

^e*Department of Chemistry and Biomolecular Science, University of Ottawa, Ottawa, K1N 6N5 Canada*

Corresponding authors are:

Mikhail S. Shchepinov, Retrotope, Inc., Los Altos, CA 94022, USA, email: shchepa65@yahoo.com
and Yuri N. Antonenko, Belozersky Institute of Physico-Chemical Biology, Lomonosov Moscow State
University, Moscow 119991, Russia, email: antonen@genebee.msu.ru

This article has been accepted for publication and undergone full peer review but has not been through the copyediting, typesetting, pagination and proofreading process, which may lead to differences between this version and the Version of Record. Please cite this article as doi: 10.1111/febs.14807

This article is protected by copyright. All rights reserved.

Accepted Article

Abstract

Autoxidation of polyunsaturated fatty acids (PUFAs) damages lipid membranes and generates numerous toxic by-products implicated in neurodegeneration, aging and other pathologies. Abstraction of bis-allylic hydrogen atoms is the rate-limiting step of PUFA autoxidation, which is inhibited by replacing bis-allylic hydrogens with deuterium atoms (D-PUFAs). In cells, the presence of a relatively small fraction of D-PUFAs among natural PUFAs is sufficient to effectively inhibit lipid peroxidation. Here, we investigate the effect of various D-PUFAs on the stability of liposomes under oxidative stress conditions. The permeability of vesicle membranes to fluorescent dyes was measured as a proxy for bilayer integrity, and the formation of conjugated dienes was monitored as a proxy for lipid peroxidation. Remarkably, both approaches reveal a similar threshold for the protective effect of D-PUFAs in liposomes. We show that protection rendered by D-PUFAs depends on the structure of the deuterated fatty acid. Our findings suggest that protection of PUFAs against autoxidation depends on the total level of deuterated bisallylic (CD₂) groups present in the lipid bilayer. However, the phospholipid containing 6,6,9,9,12,12,15,15,18,18-*d*₁₀-docosahexaenoic acid (D10-DHA) exerts a stronger protective effect than should be expected from its deuteration level. These findings further support the application of D-PUFAs as preventive/therapeutic agents in numerous pathologies that involve lipid peroxidation.

Running title: *Deuterated bisallylic groups of phospholipids stabilize liposomes*

Article type : Original Articles

Keywords: polyunsaturated fatty acids, lipid peroxidation, deuterium, reactive oxygen species, liposome leakage, conjugated dienes, bisallylic groups.

Abbreviations: LPO, lipid peroxidation; ROS, reactive oxygen species; PUFA, polyunsaturated fatty acid; D-PUFA, PUFA having bis-allylic hydrogens replaced with deuterium atoms; KIE, kinetic isotope effect; OCR, oxygen consumption rate; ALS, amyotrophic lateral sclerosis; FCS, fluorescence correlation spectroscopy; Asc, ascorbate; Ara, arachidonic acid, DHA, docosahexaenoic acid; EPA, eicosapentaenoic acid; Lin, linoleic acid; Lnn, linolenic acid; Ole, oleic acid; EtOAc, ethyl acetate; MsCl, methanesulfonyl chloride; H-LPC, hydrogenated lysophosphatidylcholine; H-Lin-PC, 1-acyl-2-linoleyl-*sn*-glycero-3-phosphatidylcholine; D2-Lin-PC, 1-acyl-2-(11,11-D₂-linoleyl)-*sn*-glycero-3-phosphatidylcholine; H-Ara-PC, 1-acyl-2-arachidonoyl-*sn*-glycero-3-phosphatidylcholine; D6-Ara-PC, 1-acyl-2-(7,7,10,10,13,13-D₆-arachidonoyl)-*sn*-glycero-3-phosphatidylcholine; H-Lnn-PC, 1-acyl-2-linolenyl-*sn*-glycero-3-phosphatidylcholine; D4-Lnn-PC, 1-acyl-2-(11,11,14,14-D₄-linolenyl)-*sn*-glycero-3-phosphatidylcholine; D2-Lnn-PC, 1-acyl-2-(14,14-D₂-linolenyl)-*sn*-glycero-3-phosphatidylcholine; D8-EPA-PC, 1-acyl-2-(7,7,10,10,13,13,16,16-D₈-eicosapentaenoyl)-*sn*-glycero-3-phosphatidylcholine; D10-DHA-PC, 1-acyl-2-(6,6,9,9,12,12,15,15,18,18-D₁₀-docosahexaenoyl)-*sn*-glycero-3-phosphatidylcholine; SRB, sulforhodamine B; D2-Lin, D4-Lnn, D6-Ara, D8-EPA and D10-DHA – linoleic acid, linolenic acid, arachidonic acid, eicosapentaenoic acid and docosahexaenoic acid, respectively, with full bis-allylic deuteration; HNE, 4-hydroxy-2-nonenal; 4-HHE, 4-hydroxy-2-hexenal; MDA, malondialdehyde.

Introduction

Polyunsaturated fatty acids (PUFAs) are essential components of lipid membranes, providing them with necessary fluidity. However, the very motif that makes PUFAs “fluid” – the “skipped” 1,4-diene moiety – also makes PUFAs susceptible to lipid peroxidation (LPO). LPO is increasingly recognized as a key contributing factor in numerous pathological events – neuronal, ocular, vascular and age related. Two features make LPO particularly pernicious: the autocatalytic radical chain reaction mechanism, and its non-enzymatic nature. The former leads to extensive damage from a single initiating event, while the latter prevents cells from evolving defences against direct control of LPO. The LPO-induced damage to living

This article is protected by copyright. All rights reserved.

Accepted Article

systems is multifaceted (Scheme 1). Compromised membrane fluidity and barrier function (Scheme 1E) occur in tandem with the formation of various carbonyl compounds (Scheme 1G) and other highly reactive species which irreversibly cross-link important biomolecules and form mutagenic DNA conjugates [1-6]. Lipid bilayer integrity is so vital to neuronal function that 5% of the total energy produced by the body is expended repairing damaged lipids in the brain [7].

To form a membrane, PUFAs (as part of phospholipids) assume a dense, uninterrupted, water-repelling regular formation, which other lipid-soluble molecules can disturb. This may contribute to the inefficiency of antioxidants in inhibiting the LPO *in vivo*, established in numerous clinical trials [3,8]. The level of antioxidants, such as tocopherols, ascorbate and reduced glutathione, in the oxidative stress-exposed PUFA-rich parts of an organism can be up-regulated by up to 40% [9]. Under stress, membranes rich in docosahexaenoic acid (DHA) could lose up to 70% of their DHA [10], which is likely due to both down regulation of the fraction of the most oxidizable PUFAs to reduce LPO, as well as loss of DHA to oxidation. Similar decreases are observed for PUFAs, in general, in animals deficient in vitamin E (vit E) [11]. Moreover, it has been suggested that certain PUFA-rich domains may have higher than average levels of vit E at normal conditions [12]. Regardless, tightly controlled delivery mechanisms cannot exceed a certain level of antioxidants in membranes, lest the structural integrity or optimal parameters of the latter be compromised. Indeed, increasing the level of vit E in model bilayers leads to decreased fluidity [13]. The reported physiological levels of tocopherols relative to fatty acid residues in lipid membranes vary depending on cellular and subcellular membrane types. The ratio of vit E to fatty acid residues can be as high as 1:130 in Golgi and lysosomal membranes [14], but more generally is around 1 tocopherol molecule per 2000 fatty acid residues [3]. However even at this high level of antioxidants, given the stochastic, random nature of ROS generation within the PUFA membranes, and the two-three orders of magnitude difference in the molar ratio of antioxidants and PUFAs, LPO cannot be completely suppressed, particularly in bilayers rich in long chain PUFAs which are easier to oxidize. Indeed, the propagation rate constants (k_p , $M^{-1} s^{-1}$) for autoxidation of PUFAs increases almost linearly with the number of bis-allylic methylene groups in a given PUFA, i.e., linoleic acid $k_p = 62$; arachidonic acid (Ara), 197 ± 13 ; eicosapentaenoic acid (EPA),

This article is protected by copyright. All rights reserved.

249 ± 16; DHA, 334 ± 37 [15]. For comparison, a monounsaturated lipid, such as oleic acid, which has no bis-allylic -CH₂- sites, has $k_p = 0.9$ [1]. In unilamellar liposomes, the values, obtained using the same method, were: Ara, 115 ± 7; EPA, 145 ± 8; DHA, 172 ± 13, thus following a pattern similar to the solution values.

Hydrogen atom transfer from carbon to oxygen is a relatively slow process, because of strong triplet repulsion or repulsion between the electrons of the CH bond and the electron of the oxygen radical. The dichotomy between LPO-associated toxicity and inefficiency of antioxidants has recently been addressed by utilizing a kinetic isotope effect (a slowing of reaction kinetics as a result of isotopic substitution) to slow down the propagation step of the LPO chain reaction [16,17]. By incorporating deuterium atoms at the bis-allylic sites of PUFAs (D-PUFAs), they become resistant to LPO, without a change in their chemical structure (Scheme 1). A useful “non-linear” feature of this approach is that LPO in cells is inhibited even when the D-PUFAs are present in membranes at relatively low (around 20 molar %) levels [18], making the approach more practical [19-25]. The exact nature of the latter effect is not fully understood, but a possibility that various pathways in a living cell might play a role cannot be ruled out.

Previous studies of this non-linear effect have involved determination of the kinetics of D-PUFA oxidation in organic solvents by monitoring oxygen consumption [26] and peroxidation by-products [18,27], thus likely bearing little relevance to processes in lipid bilayers. Studies have also been carried out in living cells [18,28], using cell survival and oxygen consumption rate (OCR) end points, but mechanistic interpretations are complicated by complex biological interactions following the initial LPO event. Such interactions may be particularly unpredictable in PUFA-rich mitochondria, where besides biochemical interactions, other confounding factors include an LPO-dependent membrane breakdown due to high membrane potential [29] and a recently reported high physiological operating temperature of mitochondria, which at 50°C may further increase the rate of LPO [30,31]. Here, we use unilamellar liposomes to test whether the LPO in simple non-living lipid membrane systems is indeed inhibited by small fractions of D-PUFAs, similar to what is observed in living cells. We find this to be the case and provide mechanistic insights into the process. The study further justifies the use of D-PUFAs as novel therapeutic agents for treatment of many retinal and neurological diseases [32-34], such as Alzheimer’s [35,36],

This article is protected by copyright. All rights reserved.

Parkinson's [37], ALS [38], in addition to many other major and orphan diseases where LPO is known to play a key detrimental role.

Results

Synthesis of phospholipids and preparation of liposomes

D2-Lin, D4-Lin [17] and D6-Ara [43] were prepared as described previously by assembling corresponding polyene chains and subjecting them to catalytic hydrogenation. Although a similar convergent synthetic strategy, based on a Wittig olefination, was developed to obtain selectively deuterated DHA species [44], D10-DHA could be prepared using the less laborious approach of catalytic H/D exchange [45]. D8-EPA was synthesized according to a newly developed procedure (Scheme 2A) based on the polyacetylene approach followed by partial hydrogenation. The efficiency of the latter was improved by using a novel catalyst, Ni-P2 poisoned with Pb^{2+} (Ni-PB2), optimized as described in the Supporting Information.

Phospholipids used in this work were synthesized from lyso-phospholipid and corresponding D- and H-PUFAs using standard protocols as shown in Scheme 2B [46,47]. Liposomes were prepared by the standard method of extrusion of lipid mixtures through a membrane filter of defined pore size [48,49].

Fluorescence Correlation Spectroscopy study of Fe/Asc-induced liposome leakage

In several recent publications [50-54], the permeability of vesicle membranes to fluorescent dyes has been studied by FCS. This approach does not require loading of liposomes with dyes at very high, self-quenching concentrations. Previously, we have shown that the addition of Fe^{2+} (5 μ M) together with ascorbate (100 μ M) brings about permeabilization of liposomes formed from the mixture of soybean phosphatidylcholine with bovine heart

This article is protected by copyright. All rights reserved.

cardiolipin, as monitored by changes in the fluorescence intensity autocorrelation function ($G(\tau)$) of the water-soluble dye SRB encapsulated in liposomes [54]. Here we studied the effect of the combination of Fe^{2+} and ascorbate on $G(\tau)$ of SRB-loaded liposomes prepared from lipid mixtures containing linoleoyl stearyl phosphatidylcholine (H-Lin-PC) as the bulk lipid (unless otherwise stated) with various contents of a series of 1-stearoyl phosphatidylcholines, bearing deuterated Lin, Lnn, Ara, EPA or DHA fatty acids at position 2 of glycerol. Importantly, SRB has been shown to be resistant to oxidative damage [49]. The amplitude of $G(\tau)$ at the limit $\tau \rightarrow 0$ is determined by the reciprocal of a mean number (N) of fluorescent particles in the observation volume [40,41]. In dye-leakage experiments, N comprises dye-loaded liposomes and free dye molecules released from liposomes. To measure $G(\tau \rightarrow 0)$ more precisely, we performed FCS experiments under stirring conditions [39]. Fig. 1A shows a time dependence of the $G(\tau)$ functions of SRB for liposomes prepared from H-Lin-PC lipids with 10 % D2-Lin-PC measured without Fe^{2+} /ascorbate (red, dark yellow, etc. lines) and after the addition of Fe /ascorbate (green, blue, etc. lines). Incubation with Fe /ascorbate led to a decrease in the $G(\tau \rightarrow 0)$ amplitude (compare, for example, green and dashed blue lines in Fig. 1A), although the decrease in the $G(\tau \rightarrow 0)$ amplitude took place even without Fe^{2+} /ascorbate. Disruption of liposomes by the addition of Triton X-100 resulted in a drop of $G(\tau \rightarrow 0)$ to nearly zero (dark green (dotted) line in Fig. 1A). Fig. 1B shows the same type of experiment carried out with liposomes having 25 % D2-Lin-PC in H-Lin-PC. In this case, the incubation with Fe^{2+} /ascorbate did not reduce the amplitude of $G(\tau \rightarrow 0)$ or reduced it to a very low extent (for example, dark yellow and blue long dashed lines). The reduction of the $G(\tau \rightarrow 0)$ amplitude apparently reflected an increase in the number of fluorescent particles due to SRB release from liposomes. It should be noted that the contribution of different fluorescent species (dye-loaded liposomes and free dye molecules released from liposomes) to $G(\tau \rightarrow 0)$ is proportional to the square of their brightness [40,41].

The $G(\tau \rightarrow 0)$ values at various periods of incubation with Fe^{2+} /ascorbate (t) can be converted into the extent of liposome leakage α using the equation [54]:

$$\alpha(t) = 1 - \sqrt{\frac{G^t(\tau \rightarrow 0)}{G^0(\tau \rightarrow 0)}} \quad (2)$$

where $G^0(\tau \rightarrow 0)$ and $G^t(\tau \rightarrow 0)$ represent $G(\tau)$ at the limit $\tau \rightarrow 0$ at the moment just before Fe^{2+} /ascorbate addition (zero time) and t min after the addition, respectively. Fig. 2A displays time courses of the extent of liposome leakage α (plus/minus Fe^{2+} /ascorbate) for liposomes having different % of D2-Lin-PC (namely, 0 %, 10 %, 25 %, and 100 %). The difference between α with and without Fe^{2+} /ascorbate was found to be high for 0 % D2-Lin-PC (red circles and red diamonds) and was very low for 100 % of the deuterated lipid (pink circles and pink diamonds).

Fe/ascorbate-induced liposome leakage and accumulation of conjugated dienes

To compare the liposome leakage induced by Fe^{2+} /ascorbate with the process of lipid peroxidation, we measured the formation of conjugated diene in the samples at 234 nm (ΔA_{234}) [42]. Fig. 2B shows the time courses of ΔA_{234} after the addition of Fe^{2+} /ascorbate to liposomes having various % of D2-Lin-PC. This parameter increased in time considerably for lipid mixtures with low percentage of deuterated D2-Lin-PC and did not increase at high content of D2-Lin-PC (Fig. 2B). Importantly, ΔA_{234} values were stable and did not increase in time without the addition of Fe^{2+} /ascorbate (data not shown).

The dependence of ΔA_{234} at $t = 10$ min (panel B) and of the difference in α in the presence/absence of Fe^{2+} /ascorbate (panel A) on the % of D2-Lin-PC are shown in Fig. 3. The curves are close to each other exhibiting a sharp decrease at low % of D2-Lin-PC leading to a very low level of ΔA_{234} and a very low value of the difference in α at about 20 % of D2-Lin-PC and higher. Fig. 4 shows the results of similar experiments with liposomes made from lipids containing arachidonic acid (H-Ara-PC) with various contents of D6-Ara-PC. Interestingly the protecting effects of D2-Lin-PC (Fig. 3) and D6-Ara-PC (Fig. 4) exerted on the corresponding

H-Lin-PC and H-Ara-PC liposomes were observed in the same concentration range of about 10 to 20 % of the deuterated lipids. These data are in good agreement with the results on the protective action of D2-Lin against LPO in membranes of yeast [18]. Surprisingly, the protective effect of 20% D2-Lin-PC in the H-Ara-PC matrix was somewhat stronger than expected, and quite close to that of D6-Ara-PC in H-Ara-PC (blue line, Fig 4B).

The extinction coefficient ϵ for conjugated dienes has been estimated to be $28000 \text{ mol}^{-1} \text{ cm}^{-1}$ at 234 nm [42]. Therefore, for the maximal ΔA of 0.05 measured after 30 minute incubation with Fe^{2+} /ascorbate (Fig. 2B), the concentration of dienes formed is around 2 μM . For 10 $\mu\text{g/ml}$ (or 10 μM) total lipids used, the level of conjugated dienes could therefore be estimated to be around 20%.

Comparison of the protective effect of D2-Lin-PC in the H-Lin-PC matrix with that of D6-Ara-PC in the H-Lin-PC matrix reveals (Fig. 5) that the protective effect of D6-Ara-PC against H-Lin-PC liposome leakage required the same concentration of D6-Ara-PC as in Fig. 4 (10-20 %), while the effect on formation of conjugated diene required a smaller amount of D6-Ara-PC (10 %).

We measured the accumulation of conjugated diene at various loadings of D10-DHA-PC in the undeuterated H-Lin-PC matrix and compared them to those measured for D8-EPA-PC, D6-Ara-PC, D4-Lnn-PC, D2-Lnn-PC and D2-Lin-PC (Fig. 6). D10-DHA-PC exhibited substantially enhanced protection from LPO compared to D6-Ara-PC and other deuterated lipids. The IC_{50} concentration was about 0.2 % for D10-DHA-PC, while IC_{50} for D8-EPA-PC was about 1.5 %, about 2 % for D6-Ara-PC, about 5 % for D4-Lnn-PC, about 22 % for D2-Lnn-PC, and about 15 % for D2-Lin-PC. Generally, increasing the number of bis-allylic CD_2 groups in a PUFA led to a stronger protective effect, more or less in a linear way. However, D10-DHA was found to be substantially more protective than should be expected from its degree of deuteration.

To assess the degree of protection elicited by D-PUFAs over a long time scale (Fig.7), we compared the accumulation of diene conjugates (ΔA_{234}) in liposomes consisting entirely of D2-Lin-PC (black curve) and ΔA_{234} in liposomes consisting of a mixture of 20 % D2-Lin-PC and 80 % H-Lin-PC (green curve) with ΔA_{234} in H-Lin-PC liposomes (red curve) as a control. While oxidation of the 100% H-PUFA liposomes occurred on the timescale of tens of minutes (red curve), the 100% D-PUFA liposomes were substantially more stable (black curve), with the oxidation timescale extending to multiple days. In case of the 20% D2-Lin-PC containing liposomes, ΔA_{234} reached saturation in about 30 hours (green curve).

Monte-Carlo simulation models threshold effect on chain length

Adding D-PUFAs to a non-deuterated membrane reduces the number of oxidatively damaged molecules, but the mechanism of the steep decline and the resulting almost complete reduction with only 20% concentration is not fully elucidated. Building a simple model of a 2D surface populated with a selected density of D-PUFAs (which would “stop” the chain propagation with varying probability) could shed light on the observations, without relying heavily on the physio-chemical effects themselves. A Monte-Carlo simulation was developed, and run while varying two different percentages, firstly the fraction of cells which were D-PUFAs that potentially terminate the chain, and secondly, the probability of the chain reaction stopping once a particular cell in the grid (a D-PUFA in the H-PUFA membrane) had been encountered. The simulation results, shown in Fig. 8, indeed reproduce the general shape and behavior of the experimental data, starting from first principles in a highly simplistic model. Interestingly, varying the % chance that the chain is stopped (i.e., 10% chance would mean that in 90% cases, the chain continues onwards) from 10 to 75% does not significantly shift the “knee” of the curves, somewhat compressing them vertically instead.

Discussion

The key propagation step of the radical chain reaction in LPO is inhibited if the abstraction-prone H-atoms at the bis-allylic positions are replaced with deuterium atoms [16]. We used phospholipids with various H- and D-PUFAs at the 2-position of the *sn*-glycero backbone to build liposomes with variable ratios of H- to D-PUFAs in lipid bilayers, and determined their stability/integrity to oxidative insult. We have previously reported that a relatively small fraction of D-PUFAs is sufficient to inhibit LPO in living cells [18,28]. The exact nature of this “20% effect” is not fully understood. The effect has been observed by monitoring oxygen consumption over the course of LPO in organic solutions of PUFAs [26]; while direct measurements of LPO end-products revealed only a 12-fold isotope effect along with some degree of LPO in the presence of 20% D-PUFAs [18,26]. In co-oxidation experiments in organic solvents, a linear relationship was observed between the total amounts of oxidation products formed and the percentage of D-PUFA, suggesting that D-PUFA did not act as an antioxidant in the co-oxidation reactions and only acted as a less reactive co-substrate in the autoxidations carried out in solution [18,27].

Studies of the non-linear protective effect in living cells using the cell survival end point [17,18] or the oxygen consumption rate (OCR) [28], while informative, are likely complicated by other factors linking LPO to cell death, so interpreting the data mechanistically is not straightforward. It is far from clear what particular stage, or product(s), of the LPO process (Scheme 1) are the most harmful to the cell and impact its survival. It was long assumed that lipid peroxides would be the most detrimental for bilayer integrity [55], while various carbonyl compounds (Scheme 1G), though toxic elsewhere, were less damaging to the membrane function. However, recent data questions this assumption, indicating that aldehydes, rather than lipid peroxides, are the group of compounds most damaging to the membrane integrity [56].

The ability to stop LPO at as early a stage as possible is highly desirable. To further elucidate the non-linear protective effect in the lipid bilayer format, but without complications elicited by biochemical pathways, we now report how D-PUFAs, in the form of synthetic phospholipids incorporated into lipid bilayers of liposomes, increase the resistance of liposomes to oxidative stress and LPO. Various methods exist for monitoring LPO. While

This article is protected by copyright. All rights reserved.

Accepted Article

monitoring carbonyls (HNE, HHE, MDA, etc) or isoprostanes only covers some aspects of the LPO process, which typically proceeds through multiple pathways (Scheme 1), fluorescent LPO markers such as BODIPY dyes have other limitations [18]. Accordingly, we chose the liposome leakage measurement [57], i.e. membrane permeabilization, as a way of monitoring the membrane damage process as a whole; and conjugated diene formation as an upstream indicator of LPO progress. The liposome leakage method [58] is a convenient way to monitor lipid bilayer integrity. However, the relatively large size of SRB may require a rather extensive degree of membrane destruction for it to leak out, which may be too substantial compared to the damage which occurs to membranes *in vivo*, even at pathological conditions. We therefore also measured the formation of conjugated dienes (Fig. 1E) [59] to more directly follow LPO.

To compare the relative inhibitory efficiency of various D-PUFAs, we tested 1-stearoyl-phosphatidylcholines containing 11,11-*d*₂-linoleic (D2-Lin-PC), 11,11,14,14-*d*₄-linolenic (D4-Lnn-PC), 14,14-*d*₂-linolenic (D2-Lnn-PC), 7,7,10,10,13,13-*d*₆-arachidonic (D6-Ara-PC), 7,7,10,10,13,13,16,16-*d*₈-eicosapentaenoic (D8-EPA-PC) and 6,6,9,9,12,12,15,15,18,18-*d*₁₀-docosahexaenoic (D10-DHA-PC) acids at position 2 of glycerol. Formation of liposomes and their subsequent processing are typically performed in air. To minimize the non-specific oxidation of H-PUFA-PCs during liposome preparation, we used H-Lin-PC as a non-deuterated bulk component of bilayers in all studies, except in Fig. 4, where H-Ara-PC was used. In the series of deuterated lipids studied here, the relative efficacy of the various D-PUFA-PCs to protect H-Lin-PC from oxidation increased with increasing number of bis-allylic CD₂ groups in the D-PUFA (assuming the LPO inhibition results in a 90% decrease in the ΔA₂₃₄ measured) as is obvious from comparing the D2-Lin-PC (at ~ 20-25% in bilayer), D2-Lnn-PC (~ 40%), D4-Lnn-PC (~ 15-20%), D6-Ara-PC (~ 10-15%) and D8-EPA-PC (~ 7-10%) series (Fig. 6). D10-DHA-PC also followed this trend. However, the protection rendered by D10-DHA-PC, suppressing LPO at as low as 1% level of incorporation in the H-Lin-PC matrix (Fig.6), was substantially stronger (10-fold stronger than for D6-Ara as measured by the conjugated diene assay) than should be expected simply from the total number of its CD₂ groups. It must be acknowledged that incorporation of DHA may lead to some physical changes in the structure of the bilayer arising from the difference in chain length between the two PUFAs (Lin: 18 carbons; DHA: 22 carbons), although the increased

number of double bonds would compensate somewhat for the length difference, by effectively “shortening” the chain. Moreover, it is known that DHA occupies a larger effective volume within the bilayer due to its curved configuration and lateral rotation, as well as other anomalous properties [60] such as its high melting point (Ara, -49.5°C; EPA, -54°C; DHA, -44°C). However, it is unclear why such physical changes would make the bilayer more resistant to oxidation.

The importance of the ratio of CD₂ to CH₂ at the bis-allylic sites in the lipid bilayer is further supported by the observation that the percentage of D6-Ara-PC, needed for protection of H-Ara-PC matrix, is similar to that found for the case of D2-Lin-PC in the H-Lin-PC matrix (Fig. 4A,B; Fig. 6) However, a surprisingly low level of D2-Lin-PC prevented the damage in H-Ara-PC matrix (Fig. 4B, blue). Furthermore, the percentage of D2-Lin-PC needed for protection of the H-Lin-PC is about two-fold higher than that of D4-Lin-PC (dark yellow and black curves in Fig.6). Increasing the total number of such “CD₂ equivalents” seems to “buffer” the chain propagating radicals, slowing them down and inhibiting LPO. This is consistent with two important earlier observations. First, mono-deuterated 11,11-D,H-Lin, bearing one H-atom and one D-atom at the same bis-allylic site protects against LPO, even though a hydrogen atom is available for abstraction. This seems to suggest a decreased reactivity of the intermediate pentadienyl and/or dienylperoxyl radicals that contain a deuterium atom (a possible role in this case of the secondary KIE was analysed in [18]). Second, a mixture of non-oxidizable oleic acid (Ole) with H-Lin (1:1) is toxic to cells while a mixture of D₂-Lin with H-Lin (1:1) is not. This suggests that D₂-Lin itself is not just a stable, non-oxidizable component of the mixture (like Ole is), but is somehow actively participating in stopping Lin from undergoing LPO (these, and other observations are discussed in detail in [18]). Hence it seems that the protective effect of D-PUFAs may have two parts: (a) a kinetic isotope effect on abstraction from the bis-allylic site, and (b) a difference in the properties of the resultant D-containing radicals as compared to H-containing radicals. The isotope effect on the atom abstraction step may be an aggregate of several effects, including both a primary and a secondary KIE. Indeed, abstraction of hydrogen from H-Lin by tocopheryl radical is 23 times faster than abstraction of D from D₂-Lin, while the corresponding intramolecular KIE for reaction of tocopheryl radical with monodeuterated 11,11-D,H-Lin is only 8.9 [27]. However, it is more challenging to

This article is protected by copyright. All rights reserved.

Accepted Article

rationalize different reactivities of the D-containing radicals compared to H-containing radicals in terms of our current understanding of the mechanism of LPO (see [62] for a comprehensive recent review). Moreover, it is difficult to explain how isotopic substitution may impact the rate of formation of products which derive from these intermediates, such as carbonyl compounds which may derive from Hock fragmentation [61], peroxy radical termination and/or alkoxy radical β -scission [56,63]. At this stage, the possibility of a secondary isotope effect on the conjugated pentadienyl system, or even some form of hyperconjugation [64] between the unpaired electron and deuterium in the intermediate peroxy, although unlikely, cannot be fully ruled out.

The threshold mechanism of protection also emerges from the Monte-Carlo simulation, performed for different “deuteration” levels, showing a similarity with the oxygen consumption rate curve for D₂-Lin:H-Lin mixtures oxidation [26], particularly the “knee” in the chain length curve (Fig.7 and SUPPORTING INFO). Oxidation of liposomes containing pure, 100% D₂-Lin-PC, was found to proceed at substantially longer (multiple days) timescale (data not shown).

A different kind of a threshold occurs when the integrity of a bilayer under oxidative stress is monitored over a longer period of time (Fig 7). Here, the 20% fraction of D₂-Lin, protective over a shorter time scale (Fig 6), holds up (green curve) in a way similar to that for a fully deuterated bilayer (black curve), but after approx. 20-24 h, succumbs to oxidative damage over a fairly narrow time window (approx. 6 h), so that by 30 h the 20% D₂-Lin bilayer is as damaged as the non-deuterated control (red curve), implying that by approx. 24 h the D-PUFA has been mostly consumed. Confirming this by mass-spectrometry may be required, while more detailed elucidation of the mechanism is likely to be complicated by a possible variable rate of initiation over time, and further difficulties arising from the fact that accumulating LPO products are often more oxidizable than the starting PUFAs.

The present study showed similarity between concentrations of deuterated phospholipids that were effective in suppressing LPO [17,18,28] and those providing protection of membrane integrity (Figs. 3 and 4). We did not quantify oxidized phospholipids or other LPO products, relying instead on the well-known correlations between membrane leakage and conjugated diene formation, “bird’s eye view” proxies of

the membrane integrity and LPO product formation, respectively [56,57,65]. At present, it remains unclear what degree of LPO is required to impair bilayer function, and also, which particular LPO products are responsible for the induction of membrane leakiness and loss of integrity. Some have suggested that lipid hydroperoxides, the primary LPO products, are responsible [55], while others have suggested that fragmentation products, such as lipid aldehydes with truncated fatty acid tails are key [56]. Therefore, the mechanism of peroxidative permeabilization of lipid membranes may vary depending on the kind of LPO induction and the presence of different protectors. Of relevance to this point could be a noticeable difference between the contents of D6-Ara-PC in the H-Lin-PC matrix that were effective in protecting against LPO (IC50 about 10 %) and SRB leakage (IC50 about 2.5 %), as seen in Fig.5, in contrast to Figs. 3 and 4.

In conclusion, the foregoing clearly demonstrates a strong protective effect of small amounts of deuterated PUFA in liposomal lipid bilayers, the phenomenon previously described in homogenous solution [26], cells [66,67,69] and living systems [18,28]. For each D-PUFA studied here, there exists a threshold percentage (e.g., about 20-25% for D2-Lin-PC and much less for D10-DHA-PC) in the H-PUFA matrix, inhibiting the LPO rate, which may be attributed to the ability of a D-PUFA-derived radical to interrupt LPO chain reactions in a lipid bilayer. The degree of protection of non-deuterated PUFAs thus correlates with the degree of deuteration, or the total number of $-CD_2-$ equivalents, present in the lipid bilayer. This useful property of D-PUFAs justifies their evaluation as potential preventive and/or therapeutic agents for various diseases in which LPO has been implicated, as attested by ongoing and completed [23] trials in neurological diseases as well as several positive studies in animal models [19-22,24,25]. Lastly, the current study suggests applications of D-PUFAs in liposome-based drug delivery approaches [68], as both the drug vehicles, and the drugs to be delivered.

Experimental procedures

Materials

Soybean lysophosphatidylcholine (Lipoid) and other commercial reagents and solvents were used as received. Chloroform was washed with water, dried with CaCl₂ and distilled over P₂O₅. ¹H (500 MHz) and ¹³C (126 MHz) NMR spectra were obtained with Bruker DRX-500 spectrometer and referenced to residual solvent signals (CDCl₃: 7.26 ppm for ¹H; CD₃OD: 4.87 ppm for ¹H and 49.00 ppm for ¹³C). Analytical thin-layer chromatography was performed on TLC Silica gel 60 F₂₅₄ (Merck). Silica gel column chromatography was performed using Merck Kieselgel 60 0.063–0.200 nm. Other reagents were from Sigma-Aldrich.

Synthesis of Ethyl 7,7,10,10,13,13,16,16-D₈-Eicosapentaenoate

1,1,4,4-D₄-Octa-2,5-diyne-1-ol (2). 250 mL round-bottom flask was charged with DMF (30 mL), CuI (10.0 g, 52 mmol), KI (9.0 g, 54 mmol) and K₂CO₃ (11.0 g, 80 mmol), then bromide **1** (10.0 g, 67 mmol) and 1,1-D₂-propargyl alcohol (89 %, 4.90 g, 75 mmol) were added. The mixture was stirred overnight under argon at room temperature and quenched with sat. NH₄Cl (80 mL), sat. NaCl (60 mL) and hexanes/EtOAc (60 mL, 3:1 v/v). After 15 min, the residue was filtered on the fine glass filter and washed with hexanes/EtOAc (3:1 v/v). The organic layer was separated, and the aqueous layer was extracted with hexanes/EtOAc (3:1 v/v, 6×50 mL). Combined organic layers were concentrated, filtered through a silica plug in hexanes/Et₂O (2:1 v/v) to give compound **2** as a colorless liquid. Yield: 6.88 g (82 %). ¹H NMR (CDCl₃, 500 MHz) δ 2.15 (q, *J* = 7.5 Hz, 2H), 2.02 (s, 1H), 1.10 (t, *J* = 7.5 Hz, 3H). ¹³C NMR (CDCl₃, 126 MHz) δ 82.56, 80.73, 78.48, 72.77, 13.90, 12.42.

1,1,4,4-D₄-1-Bromoocta-2,5-diyne (3). The solution of **2** (6.85 g, 54 mmol) in Et₂O (45 mL) was cooled to -10 °C, then Et₃N (8.7 mL, 63 mmol) and MsCl (4.80 mL, 62 mmol) were added dropwise. The reaction was stirred under -10 °C for 10 min and at rt for 30 min. To convert the obtained mesylate to bromide **3**, MgBr₂ in Et₂O was prepared by adding 1,2-dibromoethane (25.5 g, 136 mmol) in Et₂O (60 mL) to magnesium turnings (3.35 g, 140 mmol) in Et₂O (30 mL) and added to the reaction mixture. The mixture was refluxed for 30 min. The reaction was quenched with ice-cold water (30 mL), and the residue was dissolved (ether boiling!). The organic layer was separated, and the aqueous layer was extracted with Et₂O (3×50 mL). Combined organic layers were concentrated, filtered through a silica plug in hexanes to give compound **3** as a pale-yellow liquid. Yield: 9.86 g (96 %). ¹H NMR (CDCl₃, 500 MHz) δ 2.16 (q, *J* = 7.5 Hz, 2H), 1.11 (t, *J* = 7.5 Hz, 3H). ¹³C NMR (CDCl₃, 126 MHz) δ 82.80, 82.15, 75.30, 72.24, 13.92, 12.46.

1,1,4,4,7,7-D₆-Undeca-2,5,8-triyn-1-ol (4). The compound was synthesized according to the procedure for **2**, using bromide **3** (9.83 g, 52 mmol), 1,1-D₂-propargyl alcohol (89 %, 3.91 g, 60 mmol), CuI (7.6 g, 40 mmol), KI (7.0 g, 42 mmol) and K₂CO₃ (8.6 g, 62 mmol) in DMF (23 mL). The extraction was carried out using hexanes/EtOAc (3:1 v/v, 10×50 mL). Hexanes/Et₂O (1:1 v/v) was used as an eluent for chromatography on silica. Crude **4** as pale-yellow oil was mixed with hexanes and cooled at 0 °C overnight. The crystalline solid was filtered, washed with cold hexanes and dried *in vacuo*. Yield: 6.47 g (75 %). ¹H NMR (CDCl₃, 500 MHz) δ 2.15 (q, *J* = 7.5 Hz, 2H), 1.91 (s, 1H), 1.10 (t, *J* = 7.5 Hz, 3H). ¹³C NMR (CDCl₃, 126 MHz) δ 82.41, 80.06, 78.79, 75.58, 73.78, 72.98, 13.93, 12.45.

1,1,4,4,7,7-D₆-1-Bromoundeca-2,5,8-triyn (5). The compound was synthesized according to the procedure for **3**, using compound **4** (6.39 g, 39 mmol), MsCl (4.98 g, 43.5 mmol), Et₃N (6.1 mL, 43.9 mmol) in Et₂O (40 mL), Mg turnings (2.38 g, 100 mmol) in Et₂O (20 mL) and 1,2-dibromoethane (18.2 g, 97 mmol) in Et₂O (40 mL). When filtering through a silica plug, 5 % Et₂O/hexanes was used as an eluent. Yellow oil. Yield: 8.45 g (96 %). ¹H NMR (CDCl₃, 500 MHz) δ 2.16 (q, *J* = 7.5 Hz, 2H), 1.11 (t, *J* = 7.5 Hz, 3H). ¹³C NMR (CDCl₃, 126 MHz) δ 82.46, 81.41, 75.84, 75.63, 73.29, 72.92, 13.97, 12.49.

1,1,4,4,7,7,10,10-D₈-Tetradeca-2,5,8,11-tetrayn-1-ol (6). The compound was synthesized according to the procedure for **2**, using bromide **5** (8.42 g, 37 mmol), 1,1-D₂-propargyl alcohol (89 %, 2.76 g, 42 mmol), CuI (5.4 g, 28 mmol), KI (5.0 g, 30 mmol) and K₂CO₃ (6.1 g, 44 mmol) in DMF (15 mL). The extraction was carried out using hexanes/EtOAc (3:1 v/v, 7×50 mL). Crude **6** was mixed with hexanes and cooled at 0 °C overnight. The crystalline solid was filtered, washed with cold hexanes and dried *in vacuo* to give white crystals (mp 63-65 °C). Yield: 3.25 g (43 %). ¹H NMR (CDCl₃, 500 MHz) δ 2.15 (q, *J* = 7.5 Hz, 2H), 1.81 (s, 1H), 1.10 (t, *J* = 7.5 Hz, 3H). ¹³C NMR (CDCl₃, 126 MHz) δ 82.36, 79.97, 78.85, 75.39, 74.90, 74.11, 74.00, 73.04, 13.93, 12.45.

1,1,4,4,7,7,10,10-D₈-1-Bromotetradeca-2,5,8,11-tetrayne (7). The compound was synthesized according to the procedure for **3**, using compound **6** (3.20 g, 16 mmol), MsCl (2.00 g, 17.5 mmol), Et₃N (2.1 mL, 17.7 mmol) in Et₂O (20 mL), Mg turnings (0.95 g, 40 mmol) in Et₂O (8 mL) and 1,2-dibromoethane (7.33 g, 39 mmol) in Et₂O (16 mL). When filtering through a silica plug, Et₂O was used as an eluent. White crystals (mp 52-56 °C). Yield: 3.74 g (91 %). ¹H NMR (CDCl₃, 500 MHz) δ 2.16 (q, *J* = 7.5 Hz, 2H), 1.10 (t, *J* = 7.5 Hz, 3H). ¹³C NMR (CDCl₃, 126 MHz) δ 82.36, 81.28, 75.67, 75.43, 75.13, 73.94, 73.61, 73.03, 13.96, 12.47.

Ethyl 7,7,10,10,13,13,16,16-D₈-eicosa-5,8,11,14,17-pentaynoate (8). Round-bottom flask was charged with DMF (25 mL), CuI (4.9 g, 25 mmol), KI (7.3 g, 44 mmol) and K₂CO₃ (5.2 g, 38 mmol), then bromide **7** (3.69 g, 13.7 mmol) and ethyl-5-hexynoate (1.92 g, 13.7 mmol) were added. The mixture was stirred overnight under argon at room temperature and quenched with sat. NH₄Cl (55 mL), sat. NaCl (40 mL) and hexanes/EtOAc (40 mL, 4:1 v/v). After 15 min, the residue was filtered on the fine glass filter and washed with hexanes/EtOAc (4:1 v/v). The organic layer was separated, and the aqueous layer was extracted with hexanes/EtOAc (4:1 v/v, 3×30 mL). Combined organic layers were concentrated, filtered through a silica plug in 5 % EtOAc/hexanes to give compound **8** as a yellow liquid. Yield: 3.41 g (76 %). ¹H NMR (CDCl₃, 500 MHz) δ 4.11 (q, *J* = 7.2 Hz, 2H), 2.39 (t, *J* = 7.5 Hz, 2H), 2.21 (t, *J* = 7.0 Hz, 2H), 2.14 (q, *J* = 7.5 Hz, 2H), 1.78 (p, *J* = 7.2 Hz, 2H), 1.24 (t, *J* = 7.2 Hz, 3H), 1.09 (t, *J* = 7.5 Hz, 3H).

This article is protected by copyright. All rights reserved.

¹³C NMR (CDCl₃, 126 MHz) δ 82.29, 79.67, 75.29, 75.10, 74.67, 74.56, 74.49, 74.22, 74.09, 73.05, 60.43, 33.23, 23.96, 18.27, 14.33, 13.93, 12.44.

Ethyl 7,7,10,10,13,13,16,16-D₈-(all-Z)-eicosa-5,8,11,14,17-pentaenoate (9). Nickel acetate tetrahydrate (380 mg) was dissolved in 96 % EtOH (6 mL) at 50-60 °C. The flask was filled with hydrogen, and a solution of NaBH₄ in EtOH (1.57 mL), obtained from NaBH₄ (87 mg) and EtOH (2 mL) after stirring for 15 min and filtering, was added dropwise during 15 min. After 15 min, Pb(NO₃)₂ (5.8 mg) in water (40 μL), 1,2-ethylenediamine (0.47 mL,) and ester **8** (3.38 g, 10 mmol) in EtOAc (2.5 mL) were added. The mixture was stirred under hydrogen (1 atm) at 0 °C until the absorption of hydrogen stopped (3.5 h), diluted with hexanes (15 mL), glacial AcOH (0.66 mL), water (0.18 mL). Organic layer was separated; aqueous layer was extracted with hexanes/EtOAc (4:1, 4×40 mL). Combined organic layers were washed with 1M H₂SO₄, sat. NaHCO₃ and sat. NaCl (15 mL each) and dried over Na₂SO₄. Solvents were evaporated to provide a crude ester **9** (826 mg, 80 %), which was further chromatographed on AgNO₃-silica using Et₂O/hexanes mixtures (1:9, 2:8, 3:7, 4:6, 5:5, 8:2, 10:0) as an eluent to wash out the impurities. Then EtOAc was used to elute pure **9**. The sorbent was prepared by drying the mixture of SiO₂ (15 g) and AgNO₃ (4 g) in acetonitrile (10 mL) on rotary evaporator and evacuating it at 15 mmHg and 80 °C for 3 h. Pure fractions (as analyzed by TLC) were collected, evaporated and filtered through a silica plug in 10 % EtOAc in hexanes to give **9** as a colorless liquid. Yield: 330 mg (32 %). ¹H NMR (CDCl₃, 500 MHz) δ 5.37 (m, 10H), 4.12 (q, *J* = 7.1 Hz, 2H), 2.30 (t, *J* = 7.6 Hz, 2H), 2.09 (m, 4H), 1.70 (p, *J* = 7.5 Hz, 2H), 1.25 (t, *J* = 7.2 Hz, 3H), 0.97 (t, *J* = 7.6 Hz, 3H). ¹³C NMR (CDCl₃, 126 MHz) δ 173.71, 132.17, 129.16, 128.81, 128.60, 128.29, 128.16, 127.93, 127.03, 60.34, 33.84, 26.70, 24.94, 20.69, 14.38.

Synthesis of D-PUFA-containing phospholipids

Hydrogenated lysophosphatidylcholine (H-LPC, 11). Soybean lysophosphatidylcholine (3.5 g) was dissolved in MeOH (50 mL) and 5 % Pd/C (350 mg) was added to the solution. The mixture was stirred under H₂ (1 atm) for 1 h, filtered through a silica plug and cooled to 0 °C overnight. The resulting crystalline product was filtered off, washed with cold MeOH and dried *in vacuo*. The filtrate was evaporated to give another portion of product. Yield 3.39 g (95 %). ¹H NMR (CD₃OD) δ 4.28 (m, 2H), 4.17 (dd, *J* = 11.3, 4.6 Hz, 2H), 4.10 (dd, *J* = 11.3, 6.4 Hz, 2H), 4.00-3.85 (m, 3H), 3.64 (m, 2H), 3.34 (s, 2H), 3.30 (p, *J* = 1.7 Hz, 3H), 3.22 (s, 9H), 2.35 (t, *J* = 7.5 Hz, 2H), 1.61 (p, *J* = 7.2 Hz, 2H), 1.28 (m, 28H), 0.89 (t, *J* = 6.9 Hz, 3H). ¹³C NMR (CD₃OD) δ 175.34, 69.79, 67.84, 67.47, 66.22, 60.45, 54.66, 34.91, 33.09, 30.79, 30.64, 30.49, 30.45, 30.25, 26.00, 23.75, 14.46.

12a: RCOOH = linoleic acid

12b: RCOOH = 11,11-*d*₂-linoleic acid

12c: RCOOH = arachidonic acid

12d: RCOOH = 7,7,10,10,13,13-*d*₆-arachidonic acid

12e: RCOOH = linolenic acid

12f: RCOOH = 11,11,14,14-*d*₄-linolenic acid

12g: RCOOH = 14,14-*d*₂-linolenic acid

12h: RCOOH = 7,7,10,10,13,13,16,16-*d*₈-eicosapentaenoic acid

12i: RCOOH = 6,6,9,9,12,12,15,15,18,18-*d*₁₀-docosahexaenoic acid

Acylated H-LPCs (12a-i). In a typical experiment, **11** (300 mg, 0.57 mmol) was dissolved in CHCl₃ (10 mL), then fatty acid (1.15 mmol), 4-DMAP (140 mg, 1.15 mmol) and DCC (236 mg, 1.15 mmol) were added. The reaction mixture was stirred at 20 °C for 5 days, the solids were filtered off and washed with CHCl₃. The solvent was evaporated and the residue was chromatographed on silica in CHCl₃, CHCl₃ — MeOH (2:1, 1:1, 1:2) and MeOH. The pure fractions were evaporated to give the product as a colourless waxy substance. *R_f* 0.40 (CHCl₃, MeOH, conc. NH₃ 13:5:1).

1-Acyl-2-linoleyl-*sn*-glycero-3-phosphatidylcholine (H-Lin-PC, 12a). Yield 344 mg (77 %). ¹H NMR (CDCl₃) δ 5.36 (m,4H), 4.41(m,1H), 4.30(m,2H), 4.11 (dd, *J* = 12.1, 7.4 Hz, 1H), 4.00-3.85 (m, 2H), 3.76 (m,2H), 3.33 (m,9H), 2.80 (m, 2H), 2.28 (m, 4H), 2.10 (m,4H), 1.58 (m, 4H), 1.24 (m, 40H), 0.97 (m, 6H). MS (ESI) *m/z* calcd. (M+HCOO⁻) 830.61, found 830.50.

1-Acyl-2-(11,11-*d*₂-linoleyl)-*sn*-glycero-3-phosphatidylcholine (D2-Lin-PC, 12b). Yield 364 mg (81 %). ¹H NMR (CDCl₃) δ 5.36 (m, 4H), 4.41 (m, 1H), 4.30 (m, 2H), 4.11 (dd, *J* = 12.1, 7.4 Hz, 1H), 4.00-3.85 (m, 2H), 3.76 (m, 2H), 3.33 (m, 9H), 2.28 (m, 4H), 2.10 (m, 4H), 1.58 (m, 4H), 1.24 (m, 40H), 0.97 (m, 6H). MS (ESI) *m/z* calcd. (M+HCOO⁻) 832.62, found 832.42.

1-Acyl-2-arachidonoyl-*sn*-glycero-3-phosphatidylcholine (H-Ara-PC, 12c). Yield 381 mg (82 %). ¹H NMR (CDCl₃) δ 5.36 (m, 8H), 5.19 (m, 1H), 4.41 (m, 1H), 4.30 (m, 2H), 4.11 (dd, *J* = 12.1, 7.4 Hz, 1H), 4.00-3.85 (m, 2H), 3.76 (m, 2H), 3.33 (m, 9H), 2.80 (m, 6H), 2.28 (m, 4H), 2.10 (m, 4H), 1.58 (m, 4H), 1.24 (m, 38H), 0.97 (m, 6H). MS (ESI) *m/z* calcd. (M+HCOO⁻) 854.60, found 854.42.

1-Acyl-2-(7,7,10,10,13,13-*d*₆-arachidonoyl)-*sn*-glycero-3-phosphatidylcholine (D6-Ara-PC, 12d). Yield 350 mg (75 %). ¹H NMR (CDCl₃) δ 5.36 (m, 8H), 5.19 (m, 1H), 4.41 (m, 1H), 4.30 (m, 2H), 4.11 (dd, *J* = 12.1, 7.4 Hz, 1H), 4.00-3.85 (m, 2H), 3.76 (m, 2H), 3.33 (m, 9H), 2.28 (m, 4H), 2.10 (m, 4H), 1.58 (m, 4H), 1.24 (m, 38H), 0.97 (m, 6H). MS (ESI) *m/z* calcd. (M+HCOO⁻) 860.64, found 860.58.

1-Acyl-2-linolenyl-*sn*-glycero-3-phosphatidylcholine (H-Lnn-PC, 12e). Yield 330 mg (74 %). ¹H NMR (CDCl₃) δ 5.34 (m, 6H), 5.19 (m, 1H), 4.38 (m, 1H), 4.28 (m, 2H), 4.11 (dd, *J* = 12.1, 7.4 Hz, 1H), 4.00-3.85 (m, 2H), 3.76 (m, 2H), 3.33 (m, 9H), 2.80 (m, 4H), 2.28 (m, 4H), 2.10 (m, 4H), 1.58 (m, 4H), 1.24 (m, 38H), 0.97 (t, *J* = 7.5 Hz, 3H), 0.89 (t, *J* = 6.9 Hz, 3H). MS (ESI) *m/z* calcd. (M+HCOO⁻) 828.59, found 828.42.

1-Acyl-2-(11,11,14,14-D₄-linolenyl)-sn-glycero-3-phosphatidylcholine (d₄-Lnn-PC, 12f). Yield 410 mg (90 %). ¹H NMR (CDCl₃) δ 5.34 (m, 6H), 5.19 (m, 1H), 4.38 (m, 1H), 4.28 (m, 2H), 4.11 (dd, *J* = 12.1, 7.4 Hz, 1H), 4.00-3.85 (m, 2H), 3.76 (m, 2H), 3.33 (m, 9H), 2.28 (m, 4H), 2.05 (m, 4H), 1.58 (m, 4H), 1.24 (m, 38H), 0.97 (t, *J* = 7.5 Hz, 3H), 0.89 (t, *J* = 6.9 Hz, 3H). MS (ESI) *m/z* calcd. (M+HCOO⁻) 832.61, found 832.42.

1-Acyl-2-(14,14-D₂-linolenyl)-sn-glycero-3-phosphatidylcholine (d₂-Lnn-PC, 12g). Yield 366 mg (81 %). ¹H NMR (CDCl₃) δ 5.34 (m, 6H), 5.19 (m, 1H), 4.38 (m, 1H), 4.28 (m, 2H), 4.11 (dd, *J* = 12.1, 7.4 Hz, 1H), 4.00-3.85 (m, 2H), 3.76 (m, 2H), 3.39 (m, 9H), 2.80 (m, 2H), 2.28 (m, 4H), 2.10 (m, 4H), 1.58 (m, 4H), 1.24 (m, 38H), 0.97 (t, *J* = 7.5 Hz, 3H), 0.89 (t, *J* = 6.9 Hz, 3H). MS (ESI) *m/z* calcd. (M+HCOO⁻) 830.60, found 830.42.

1-Acyl-2-(7,7,10,10,13,13,16,16-D₈-eicosapentaenoyl)-sn-glycero-3-phosphatidylcholine (d₈-EPA-PC, 12h). Yield 371 mg (80 %). ¹H NMR (CDCl₃) δ 5.36 (m, 10H), 5.19 (m, 1H), 4.39 (dd, *J* = 12.0, 2.9 Hz, 1H), 4.28 (m, 2H), 4.11 (dd, *J* = 12.1, 7.3 Hz, 1H), 4.00-3.85 (m, 2H), 3.76 (m, 2H), 3.33 (m, 9H), 2.31 (t, *J* = 7.6 Hz, 2H), 2.26 (t, *J* = 7.6 Hz, 2H), 2.10 (m, 2H), 1.66 (m, 2H), 1.58 (m, 2H), 1.24 (m, 28H), 0.97 (t, *J* = 7.5 Hz, 3H), 0.89 (t, *J* = 6.9 Hz, 3H). MS (ESI) *m/z* calcd. (M+HCOO⁻) 860.64, found 862.50.

1-Acyl-2-(6,6,9,9,12,12,15,15,18,18-d₁₀-docosahexaenoyl)-sn-glycero-3-phosphatidylcholine (D10-DHA-PC, 12i). Yield 390 mg (81%). ¹H NMR (CDCl₃) δ 5.36 (m,12H), 5.19 (m,1H), 4.38 (m, 1H), 4.28 (m, 2H), 4.12 (dd, *J* = 12.1, 7.4 Hz, 1H), 4.00-3.85 (m,2H), 3.76 (m, 2H), 3.67 (m, 4H), 3.33 (m, 9H), 2.36 (m, 4H), 2.28 (m, 2H), 1.58 (m, 2H), 1.24 (m,28H), 0.97 (t, *J* = 7.5 Hz, 3H), 0.89 (t, *J* = 6.9 Hz, 3H). MS (ESI) *m/z* calcd. (M+HCOO⁻) 888.67, found 889.58.

Preparation of liposomes

Plain and dye-loaded unilamellar liposomes were prepared by evaporation under a stream of nitrogen of a 2 % solution of a mixture of lipids in chloroform followed by hydration with a buffer solution containing a fluorescent marker for dye-loaded liposomes. We used 5 mg of appropriate phosphatidylcholine mixture and added 0.5 ml of 1 mM sulforhodamine B (SRB) in 100 mM KCl, 10 mM Tris, 10 mM MES, pH 7.4. The mixture was vortexed, passed through several cycles of freezing and thawing, and extruded through 0.1- μm pore size Nucleopore polycarbonate membranes using an Avanti Mini-Extruder. The unbound fluorescent marker was then removed by passage through a Sephadex G-50 coarse column with a buffer solution containing 100 mM KCl, 10 mM Tris, 10 mM MES, pH 7.4.

Fluorescence correlation spectroscopy

The custom-made setup was described previously [39]. Briefly, fluorescence excitation and detection utilized a Nd:YAG solid state laser with a 532-nm beam attached to an Olympus IMT-2 epifluorescent inverted microscope equipped with a 40x, NA 1.2 water immersion objective (Carl Zeiss, Jena, Germany). The fluorescence light passed through an appropriate dichroic beam splitter and a long-pass filter and was imaged onto a 50- μm core fiber coupled to an avalanche photodiode (SPCM-AQR-13-FC, PerkinElmer Optoelectronics, Vaudreuil, Quebec, Canada). The output signal was sent to a PC using a fast interface card (Flex02-01D/C, Correlator.com, Bridgewater, NJ). Data acquisition time was 30 s. Fluorescence was recorded from the confocal volume located at about 50 μm above the coverslip surface with 50 μl of the buffer solution added. Most of the data were collected under the conditions of stirring liposome dispersions with a paddle-shaped 3-mm plastic bar rotated at 600 rpm. To calibrate the setup, we recorded the fluorescence autocorrelation function of Rhodamine 6G solution. Assuming the diffusion coefficient of the dye to be $2.5 \times 10^{-6} \text{ cm}^2/\text{s}$, the value of the confocal radius $\omega=0.42 \mu\text{m}$ was obtained. The correlated

fluorescence emission signals were fitted to the three-dimensional autocorrelation function [40,41].

$$G(\tau) = \frac{1}{N} \left(\frac{1}{1 + \frac{\tau}{\tau_D}} \right) \left(\frac{1}{\sqrt{1 + \frac{\omega^2 \tau}{z_0^2 \tau_D}}} \right) \quad (1)$$

with τ_D being the characteristic correlation time during which a molecule resides in the observation volume of radius ω and length z_0 , given by $\tau_D = \omega^2/4D$, where D is the diffusion coefficient, N is the mean number of fluorescent particles in the confocal volume. The amplitude of the autocorrelation function is inversely proportional to the number of fluorescent particles ($N=1/G(\tau \rightarrow 0)$), but is independent of the fluorescence intensity of a single particle (in a system of identical particles) and therefore does not depend on the number of fluorophores per vesicle. Particles can be any fluorescent “point objects” in comparison to the dimension of the observation volume (i.e. about 1 micrometer). Therefore, particles can be single molecules of dye (i.e. SRB), as well as liposomes carrying different numbers of dye molecules. Initially (before the leakage induction) the system has a limited number of particles per observation volume comprising predominantly several liposomes loaded with the dye. After the leakage, the number of particles increases substantially, because every liposomal particle produces thousands of particles of free dye leading to a significant decrease of the parameter $G(\tau \rightarrow 0)$.

Conjugated diene assay

The level of conjugated dienes was determined from the absorption at 234 nm [42]. The UV spectrum of the liposome suspension was measured with a CM 2203 spectrophotometer (SOLAR, Belarus) at various time intervals after the addition of 5 μM FeSO_4 and 100 μM ascorbate, subtracting the initial spectrum at time zero. The peak of conjugated dienes was seen as a shoulder in the broad band of ascorbate. As a measure of the level of diene conjugates, the absorbance value at 234 nm was taken from which the

Accepted Article

averaged absorbance at 228 nm and 240 nm was subtracted, namely $\Delta A_{234} = A_{234} - (A_{228} + A_{240})/2$. The data points represented Mean \pm S.D. of at least three independent experiments.

Monte Carlo simulation

A simulation program that roughly modeled the effect of D-PUFAs on the lipid chain reaction was written using Processing 3.0. A rectangular grid with 400 x 400 cells was populated randomly with given concentration of D-PUFA. The chain reaction was initiated at the central cell, thereafter a 2D random walk simulation proceeded to one of the eight neighboring cells with equiprobability, damaging encountered H-PUFAs with 100% probability until a D-PUFA was hit. The chain was then randomly stopped based on a parameter ("strength", a parameter that represents the probability that the chain terminates) of the model, which embodies a combination of those properties that quench the propagating peroxy radical. An average of 100 runs was performed for each set of parameters.

Acknowledgements

We are very grateful to Prof Cathy F. Clarke (UCLA, USA) and Prof Derek Pratt (Ottawa University, Canada) for providing their insights on the manuscript. This work was financially supported by the Russian Science Foundation Grant 16-14-10025.

Author Contributions:

MSS initiated the project; YNA and MSS designed the experiments, and YNA, MSS and DAP interpreted the data; AMF performed biophysical and biochemical experiments; VVS and DV designed schemes of synthesis of D-PUFA-containing lipids; MAF, AVB and OLS performed synthesis of the deuterated lipids; HJS performed the Monte-Carlo simulation; MSS, YNA, EAK and DAP wrote the manuscript.

This article is protected by copyright. All rights reserved.

Disclaimers

H.J. Saal and M.S. Shchepinov are employed by, and hold stocks in Retrotope, Inc.

References

1. Yin H, Xu L, Porter NA (2011) Free radical lipid peroxidation: mechanisms and analysis. *Chem Rev* **111**, 5944–5972.
2. Esterbauer H, Schaur RJR, Zollner H (1991) Chemistry and biochemistry of 4-hydroxynonenal, malonaldehyde and related aldehydes. *Free Radic Biol Med* **11**, 81–128.
3. Halliwell B, Gutteridge JMC (2007) *Free Radicals in Biology and Medicine*, Oxford University Press, New York.
4. Roberts LJ, Fessel JP (2004) The biochemistry of the isoprostane, neuroprostane, and isofuran pathways of lipid peroxidation. *Chem Phys Lipids* **128**, 173–186, doi: 10.1016/j.chemphyslip.2003.09.016.
5. Negre-Salvayre A, Coatrieux C, Inguenau C, Salvayre R (2008) Advanced lipid peroxidation end products in oxidative damage to proteins: potential role in diseases and therapeutic prospects for the inhibitors. *Br J Pharmacol* **153**, 6–20.
6. Blair IA (2008) DNA adducts with lipid peroxidation products. *J Biol Chem* **283**, 15545–15549.
7. Brenna JT, Carlson SE (2014) Docosahexaenoic acid and human brain development: evidence that a dietary supply is needed for optimal development. *J Human Evol* **77**, 99–106, doi: 10.1016/j.jhevol.2014.02.017.
8. Kamat CD, Gadal S, Mhatre M, Williamson KS, Pye QN, Hensley K (2008) Antioxidants in central nervous system disease: preclinical promise and translational challenges. *J Alzheimers Dis* **15**, 473–493.
9. Penn JS, Naash MI, Anderson RE (1987) Effect of light history on retinal antioxidants and light damage susceptibility in the rat. *Exp Eye Res* **44**, 779–788.
10. Penn JS, Anderson RE (1987) Effect of light history on rod outer-segment membrane composition in the rat. *Exp Eye Res* **44**, 767–778.

11. Zhang Y, Turunen M, Appelkvist EL (1996) Restricted uptake of dietary coenzyme Q is in contrast to the unrestricted uptake of α -tocopherol into rat organs and cells. *J Nutr* **126**, 2089–2097, doi: 10.1093/jn/126.9.2089.
12. Atkinson J, Harroun T, Wassall SR, Stillwell W, Katsaras J (2010) The location and behaviour of α -tocopherol in membranes. *Mol Nutr Food Res* **54**, 641–665, doi: 10.1002/mnfr.200900439.
13. Urano S, Yano K, Matsuo M (1988) Membrane-stabilizing effect of vitamin E: effect of alpha-tocopherol and its model compounds on fluidity of lecithin liposomes. *Biochem Biophys Res Commun* **150**, 469–475.
14. Wang X, Quinn PJ (2000) The location and function of vitamin E in membranes. *Mol Membr Biol* **17**, 143–156.
15. Xu L, Davis TA, Porter NA (2009) Rate constants for peroxidation of polyunsaturated fatty acids and sterols in solution and in liposomes. *J Am Chem Soc* **131**, 13037–13044, doi: 10.1021/ja9029076.
16. Shchepinov MS (2007) Reactive oxygen species, isotope effect, essential nutrients, and enhanced longevity. *Rejuvenation Res* **10**, 47–59, doi: 10.1089/rej.2006.0506.
17. Hill S, Hirano K, Shmanai VV, Marbois BN, Vidovic D, Bekish AV, Kay B, Tse V, Fine J, Clarke CF, Shchepinov MS (2011) Isotope-reinforced polyunsaturated fatty acids protect yeast cells from oxidative stress. *Free Radic Biol Med* **50**, 130–138, doi: 10.1016/j.freeradbiomed.2010.10.690.
18. Hill S, Lamberson CR, Xu L, To R, Tsui HS, Shmanai VV, Bekish AV, Awad AM, Marbois BN, Cantor CR, Porter NA, Clarke CF, Shchepinov MS (2012) Small amounts of isotope-reinforced polyunsaturated fatty acids suppress lipid autoxidation. *Free Radic Biol Med* **53**, 893–906, doi: 10.1016/j.freeradbiomed.2012.06.004.
19. Shchepinov MS, Chou VP, Pollock E, Langston JW, Cantor CR, Molinari RJ, Manning-Bog AB (2011) Isotopic reinforcement of essential polyunsaturated fatty acids diminishes nigrostriatal degeneration in a mouse model of Parkinson's disease. *Toxicol Lett* **207**, 97–103, doi: 10.1016/j.toxlet.2011.07.020.
20. Berbee JFP, Mol IM, Milne GL, Pollock E, Hoeke G, Lutjohann D, Monaco C, Rensen PCN, van der Ploeg LHT, Shchepinov MS (2017) Deuterium-reinforced polyunsaturated fatty acids protect against atherosclerosis by lowering lipid peroxidation and hypercholesterolemia. *Atherosclerosis* **264**, 100–107, doi: 10.1016/j.atherosclerosis.2017.06.916.
21. Elharram A, Czegledy NM, Golog M, Milne GL, Pollock E, Bennett BM, Shchepinov MS (2017) Deuterium-reinforced polyunsaturated fatty acids improve cognition in a

- mouse model of sporadic Alzheimer's disease. *FEBS J* **284**, 4083–4095, doi: 10.1111/febs.14291.
22. Raefsky SM, Furman R, Milne G, Pollock E, Axelsen P, Mattson MP, Shchepinov MS (2018) Deuterated polyunsaturated fatty acids reduce brain lipid peroxidation and hippocampal amyloid beta-peptide levels, without discernible behavioural effects in an APP/PS1 mutant transgenic mouse model of Alzheimer's disease. *Neurobiol Aging* **66**, 165–176, doi: 10.1016/j.neurobiolaging.2018.02.024.
23. Zesiewicz T, Heerinckx F, De Jager R, Omidvar O, Kilpatrick M, Shaw J, Shchepinov MS (2018) Randomized, clinical trial of RT001: early signal of efficacy in Friedreich's ataxia. *Mov Disord* **33**, 1000–1005, doi: 10.1002/mds.27353.
24. Hatami A, Zhu C, Relación-Gines A, Elias C, Galstyan A, Jun M, Milne G, Cantor CR, Chesselet MF, Shchepinov MS (2018) Deuterium-reinforced linoleic acid lowers lipid peroxidation and mitigates cognitive impairment in the Q140 knock in mouse model of Huntington's disease. *FEBS J*, doi: 10.1111/febs.14590.
25. Angelova PR, Horrocks MH, Klenerman D, Gandhi S, Abramov AY, Shchepinov MS (2015) Lipid peroxidation is essential for α -synuclein-induced cell death. *J Neurochem* **133**, 582–589, doi: 10.1111/jnc.13024.
26. Shchepinov MS, Roginsky VA, Brenna JT, Molinari RJ, To R, Tsui H, Clarke CF, Manning-Bog AB (2014) Deuterium protection of polyunsaturated fatty acids against lipid peroxidation: a novel approach to mitigating mitochondrial neurological diseases. In *Omega 3 Fatty Acids in Brain and Neurological Health* (R.S. Watson & F. De Meester, eds.), pp. 373–383, Elsevier Academic Press, Amsterdam.
27. Lamberson CR, Xu L, Muchalski H, Montenegro-Burke JR, Shmanai VV, Bekish AV, McLean JA, Clarke CF, Shchepinov MS, Porter NA (2014) Unusual kinetic isotope effects of deuterium reinforced polyunsaturated fatty acids in tocopherol-mediated free radical chain oxidations. *J Am Chem Soc* **136**, 838–841, doi: 10.1021/ja410569g.
28. Andreyev AY, Tsui HS, Milne GL, Shmanai VV, Bekish AV, Fomich MA, Pham MN, Nong Y, Murphy AN, Clarke CF, Shchepinov MS (2015) Isotope-reinforced polyunsaturated fatty acids protect mitochondria from oxidative stress. *Free Radic Biol Med* **82**, 63–72, doi: 10.1016/j.freeradbiomed.2014.12.023.
29. Vladimirov UA, Parnev OM, Annaberdyeva EM, Putvinskij AB, Putschkova TV (1984) Electric Stability of Mitochondrial Membranes. *Biol Membr (Rus)* **4**, 428-434.
30. Chretien D, Benit P, Ha HH, Keipert S, El-Khoury R, Chang YT, Jastroch M, Jacobs HT, Rustin P, Rak M (2018) Mitochondria are physiologically maintained at close to 50°C. *PLoS Biol* **16(1)**, e2003992, doi: 10.1371/journal.pbio.2003992.

31. Lane N (2018) Hot mitochondria? *PLoS Biol* **16(1)**, e2005113, doi: 10.1371/journal.pbio.2005113.
32. Reed TT (2011) Lipid peroxidation and neurodegenerative disease. *Free Radic Biol Med* **51**, 1302–1319, doi: 10.1016/j.freeradbiomed.2011.06.027.
33. Yagi K (1987) Lipid peroxides and human diseases. *Chem Phys Lipids* **45**, 337–351.
34. Anderson RE, Rapp LM, Wiegand RD (1984) Lipid peroxidation and retinal degeneration. *Curr Eye Res* **3**, 223–227.
35. Sayre LM, Zelasko DA, Harris PLR, Perry G, Salomon RG, Smith MA (1997) 4-Hydroxynonenal-derived advanced lipid peroxidation end products are increased in Alzheimer's disease. *J. Neurochem* **68**, 2092–2097.
36. Butterfield DA, Lauderback CM (2002) Lipid peroxidation and protein oxidation in Alzheimer's disease brain: potential causes and consequences involving amyloid beta-peptide-associated free radical oxidative stress. *Free Radic Biol Med* **32**, 1050–1060.
37. Dexter DT, Carter CJ, Wells FR, Javoy-Agid F, Agid Y, Lees A, Jenner P, Marsden CD (1989) Basal lipid peroxidation in Substantia Nigra is increased in Parkinson's disease. *J Neurochem* **52**, 381–389.
38. Pedersen WA, Fu W, Keller JN, Markesbery WR, Appel S, Smith RG, Kasarskis E, Mattson MP (1998) Protein modification by the lipid peroxidation product 4-HNE in the spinal cords of amyotrophic lateral sclerosis patients. *Annals Neurol* **44**, 819–824.
39. Perevoshchikova IV, Zorov DB, Antonenko YN (2008) Peak intensity analysis as a method for estimation of fluorescent probe binding to artificial and natural nanoparticles: tetramethylrhodamine uptake by isolated mitochondria. *Biochim Biophys Acta* **1778**, 2182–2190. doi: 10.1016/j.bbamem.2008.04.008.
40. Hess ST, Huang S, Heikal AA, Webb WW (2002) Biological and chemical applications of fluorescence correlation spectroscopy: a review. *Biochemistry* **41**, 697–705.
41. Krichevsky O, Bonnet G (2002) Fluorescence correlation spectroscopy: the technique and its applications. *Rep Prog Phys* **65**, 251–297, doi: 10.1088/0034-4885/65/2/203.
42. Yamamoto Y, Niki E, Kamiya Y, Shimasaki H (1984) Oxidation of lipids. 7. Oxidation of phosphatidylcholines in homogeneous solution and in water dispersion. *Biochim Biophys Acta* **795**, 332–340.
43. Fomich MA, Bekish AV, Vidovic D, Lamberson CR, Lysenko IL, Lawrence P, Brenna JT, Sharko OL, Shmanai VV, Shchepinov MS (2016) Full library of (bis-allyl)-deuterated

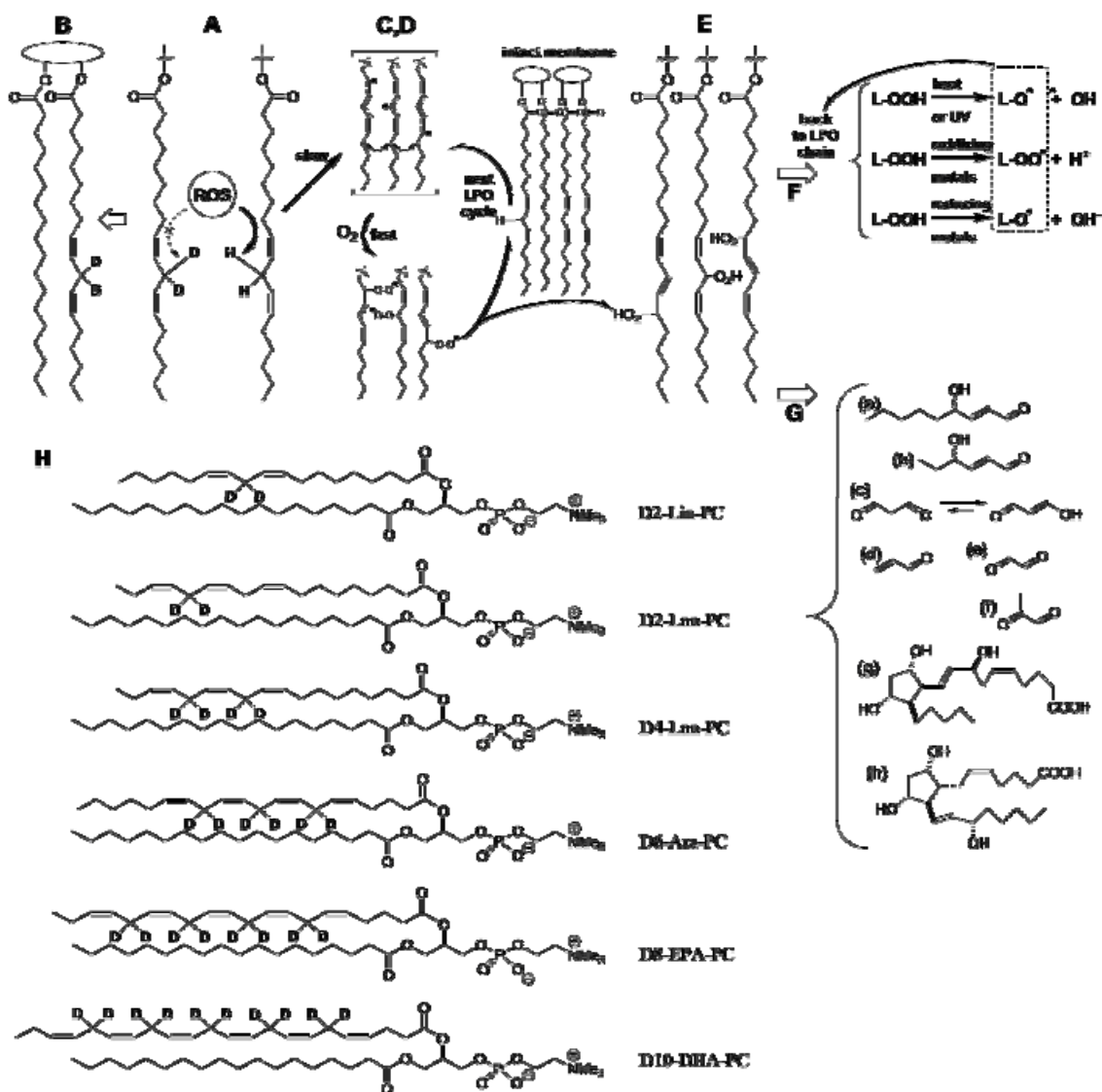
- arachidonic acids: synthesis and analytical verification. *Chemistry Select* **1**, 4758–4764, doi: 10.1002/slct.201600955.
44. Rosell M, Villa M, Durand T, Galano J-M, Vercauteren J, Crauste C (2017) Total syntheses of two bis-allylic-deuterated DHA analogues. *Asian J Org Chem* **6(3)**, 322–334, doi: 10.1002/ajoc.201600565.
45. Smarun AV, Petkovic M, Shchepinov MS, Vidovic D (2017) Site-specific deuteration of polyunsaturated alkenes. *J Org Chem* **82**, 13115–13120. doi: 10.1021/acs.joc.7b02169.
46. Neises B, Steglich W (1978) Simple method for esterification of carboxylic acids. *Angew Chem Internat Ed* **17**, 522–524.
47. Nishimura S (2001) Hydrogenation of Alkenes. In *Handbook of Heterogeneous Catalytic Hydrogenation for Organic Synthesis*, pp. 64–147, John Wiley & Sons, Inc., NY.
48. Olson F, Hunt CA, Szoka FC, Vail WJ, Papahadjopoulos D (1979) Preparation of liposomes of defined size distribution by extrusion through polycarbonate membranes. *Biochim Biophys Acta* **557**, 9–23.
49. Pashkovskaya A, Kotova E, Zorlu Y, Dumoulin F, Ahsen V, Agapov I, Antonenko Y (2010) Light-triggered liposomal release: membrane permeabilization by photodynamic action. *Langmuir* **26**, 5726–5733, doi: 10.1021/la903867a.
50. Yu L, Ding JL, Ho B, Feng SS, Wohland T (2008) Investigation of the mechanisms of antimicrobial peptides interacting with membranes by fluorescence correlation spectroscopy. *The Open Chemical Physics Journal* **1**, 62–80, doi: 10.2174/1874412500801010062.
51. Blicher A, Wodzinska K, Fidorra M, Winterhalter M, Heimburg T (2009) The temperature dependence of lipid membrane permeability, its quantized nature, and the influence of anesthetics. *Biophys J* **96**, 4581–4591, doi: 10.1016/j.bpj.2009.01.062.
52. Sorochkina AI, Kovalchuk SI, Omarova EO, Sobko AA, Kotova EA, Antonenko YN (2013) Peptide-induced membrane leakage by lysine derivatives of gramicidin A in liposomes, planar bilayers, and erythrocytes. *Biochim Biophys Acta* **1828**, 2428–2435. doi: 10.1016/j.bbamem.2013.06.018.
53. Kristensen K, Henriksen JR, Andresen TL (2014) Quantification of leakage from large unilamellar lipid vesicles by fluorescence correlation spectroscopy. *Biochim Biophys Acta* **1838**, 2994–3002, doi: 10.1016/j.bbamem.2014.08.007.

54. Firsov AM, Kotova EA, Korepanova EA, Osipov AN, Antonenko YN (2015) Peroxidative permeabilization of liposomes induced by cytochrome *c*/cardiolipin complex. *Biochim Biophys Acta* **1848**, 767–774, doi: 10.1016/j.bbamem.2014.11.027.
55. Dobretsov GE, Borschevskaya TA, Petrov VA, Vladimirov YA (1977) The increase of phospholipid bilayer rigidity after lipid peroxidation. *FEBS Lett* **84**, 125–128.
56. Bacellar IOL, Oliveira MC, Dautas LS, Costa EB, Junqueira HC, Martins WK, Durantini, G. Cosa, P. Di Mascio, M. Wainwright, R. Miotto, R.M. Cordeiro, S. Miyamoto AM, Baptista MS (2018) Photosensitized membrane permeabilization requires contact-dependent reactions between photosensitizer and lipids. *J Am Chem Soc* **140**, 9606–9615, doi: 10.1021/jacs.8b05014.
57. Kunimoto M, Inoue K, Nojima S (1981) Effect of ferrous ion and ascorbate-induced lipid peroxidation on liposomal membranes. *Biochim Biophys Acta* **646**, 169–178.
58. Weinstein JN, Klausner RD, Innerarity T, Ralston E, Blumenthal R (1981) Phase transition release, a new approach to the interaction of proteins with lipid vesicles. Application to lipoproteins. *Biochim. Biophys. Acta* **647**, 270–284.
59. Esterbauer H, Striegl G, Puhl H, Rotheneder M (1989) Continuous monitoring of in vitro oxidation of human low density lipoprotein. *Free Radic Res Commun* **6**, 67–75.
60. Crawford MA, Broadhurst CL, Guest M, Nagar A, Wang Y, Ghebremeskel K, Schmidt WF (2013) A quantum theory for the irreplaceable role of docosahexaenoic acid in neural cell signaling throughout evolution. *Prostaglandins Leukotrienes Essent Fatty Acids* **88**, 5–13, doi: 10.1016/j.plefa.2012.08.005.
61. Pryor WA, Porter NA (1990) Suggested mechanisms of the production of 4-HNE from the autoxidation of polyunsaturated fatty acids. *Free Radic Biol Med* **8**, 541–543.
62. Zielinski ZAM, Pratt DA (2017) Lipid Peroxidation: Kinetics, Mechanisms, and Products. *J Org Chem* **82**, 2817–2825, doi: 10.1021/acs.joc.7b00152.
63. Russell GA (1957) Deuterium-isotope effects in the autoxidation of aralkyl hydrocarbons, Mechanism of the interaction of peroxy radicals. *J Am Chem Soc* **79**, 3871–3877.
64. Shiner VJ Jr. (1959) Deuterium isotope effects and hyperconjugation. *Tetrahedron* **5**, 243–252.
65. Agmon E, Solon J, Bassereau P, Stockwell BR (2018) Modeling the effects of lipid peroxidation during ferroptosis on membrane properties. *Scientific Reports* **8**, 5155–5170, doi: 10.1038/s41598-018-23408-0.

66. Yang WS, Stockwell BR (2016) Ferroptosis: death by lipid peroxidation. *Trends Cell Biol* **26**, 165–176, doi: 10.1016/j.tcb.2015.10.014.
67. Yang WS, Kim KJ, Gaschler MM, Patel M, Shchepinov MS, Stockwell BR (2016) Peroxidation of polyunsaturated fatty acids drives ferroptosis. *Proc Natl Acad Sci USA* E4966-E4975, doi: 10.1073/pnas.1603244113.
68. Allen TM, Cullis PR (2013) Liposomal drug delivery systems: From concept to clinical applications. *Adv Drug Deliv Rev* **65**, 36–48, doi: 10.1016/j.addr.2012.09.037.
69. Shah R, Shchepinov MS, Pratt DA (2018) Resolving the role of lipoxygenases in the initiation and execution of ferroptosis. *ACS Cent. Sci.* **4**, 387-396, doi: 10.1021/acscentsci.7b00589.

Supporting information

Additional Supporting Information may be found online in the supporting information tab for this article.



Scheme 1. Protective effect of D-PUFAs on LPO. **A**, D-PUFAs inhibit the rate-limiting step of reactive oxygen species (ROS)-driven abstraction off a bis-allylic site. **B**, A lipid bilayer that incorporates D-PUFAs (shown, n-6 PUFAs D2-linoleic and D2-arachidonic acids) is resistant to LPO. **C**, ROS-driven hydrogen abstraction off a bis-allylic site (**A**) generates resonance-stabilized free radicals (**C**), which quickly react with abundant molecular oxygen to form lipid peroxy radicals (**D**). These newly formed ROS species (L-OO[•]) abstract hydrogen off a neighboring PUFA (turning themselves into lipid peroxides (LOOH) (**E**)), thus sustaining the chain reaction of LPO, which is eventually terminated by a chain-terminating anti-oxidant or homologous recombination (not shown). (**F**), Linoleic acid or 11,11-D₂-linoleic acid (18:2,n-6) used in this study (a), are enzymatically converted into arachidonic acid and 13,13-D₂-

arachidonic acid (20:4,n-6). A non-deuterated alpha-linolenic acid (18:3,n-3) was used both in experimental and control diets. Once ingested, it is enzymatically converted into higher n-3 PUFAs, EPA and DHA (not shown). Lipid peroxides (**E**), which have greater volume and are more hydrophilic than non-oxidized lipids. Peroxides formed may decompose through multiple pathways back into chain-initiating radicals (**F**), which can initiate new chains. Eventually, peroxides decay into numerous non-radical species (**G**) such as reactive carbonyls, including 4-HNE (a), 4-HHE (b), and malondialdehyde, which predominantly exists in one tautomeric form (c), acrylic aldehyde (d), oxalic aldehyde (e), and methylglyoxal (f). Other classes of products include arachidonic acid-derived isoprostanes (g; iPF_{2α}-IV, or 8-F₂-IsoP, which is one of 64 different isomers), as well as PGF_{2α} (h), a prostaglandin that can be produced both enzymatically and non-enzymatically.

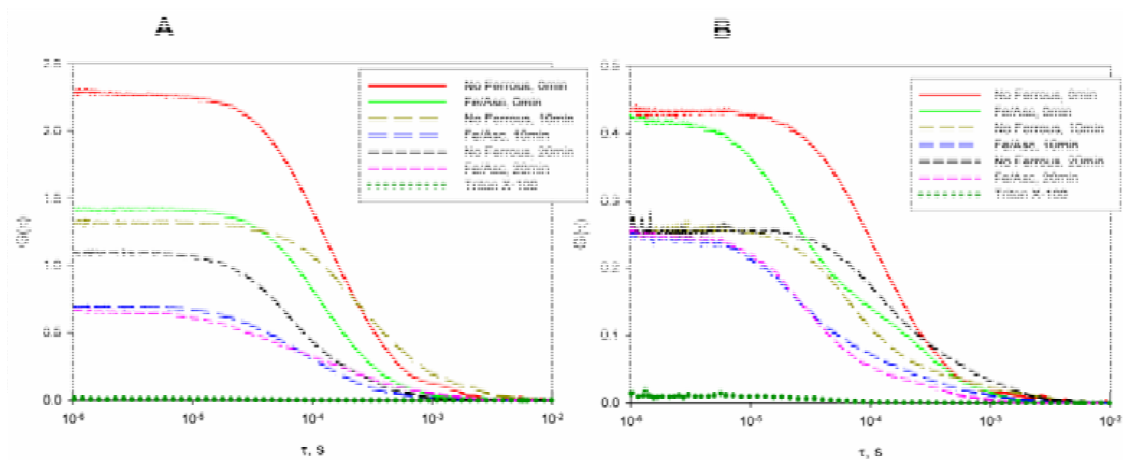


Figure 1. Fe^{2+} /ascorbate-induce leakage of SRB from liposomes made from 90 % H-Lin-PC/10 % D2-Lin-PC (A) or 75 % H-Lin-PC/25 % D2-Lin-PC (B). Typical autocorrelation functions of SRB-loaded liposomes differing in the time of incubation with FeSO_4 (5 μM) and ascorbate (100 μM) and corresponding controls without Fe^{2+} /ascorbate. Solid lines corresponded to zero time of incubation, long-dashed and short-dashed lines to 10 min and to 20 min of incubations, respectively. Autocorrelation functions in the presence of Triton-X100 are dotted lines. The buffer contained 100 mM KCl, 10 mM Tris, 10 mM MES, pH 7.4. Lipid concentration, 10 $\mu\text{g}/\text{ml}$.

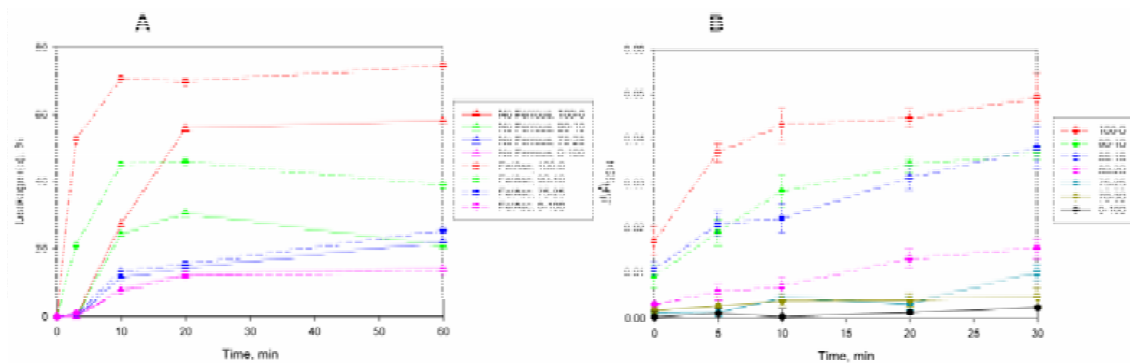


Figure 2. Typical kinetics of SRB leakage (A) and accumulation of diene conjugates (B) in liposomes with various contents of D2-Lin-PC lipid in the undeuterated H-Lin-PC matrix. The parameter α was calculated according to Eqn.2. Diene conjugates were estimated from the absorbance at 234 nm. Measurements were carried out after various periods of incubation with FeSO_4 ($5 \mu\text{M}$) and ascorbate ($100 \mu\text{M}$) as well as in controls without Fe^{2+} /ascorbate. The buffer contained 100 mM KCl, 10 mM Tris, 10 mM MES, pH 7.4. Lipid concentration, $10 \mu\text{g}/\text{ml}$. The data points represented Mean \pm S.D.

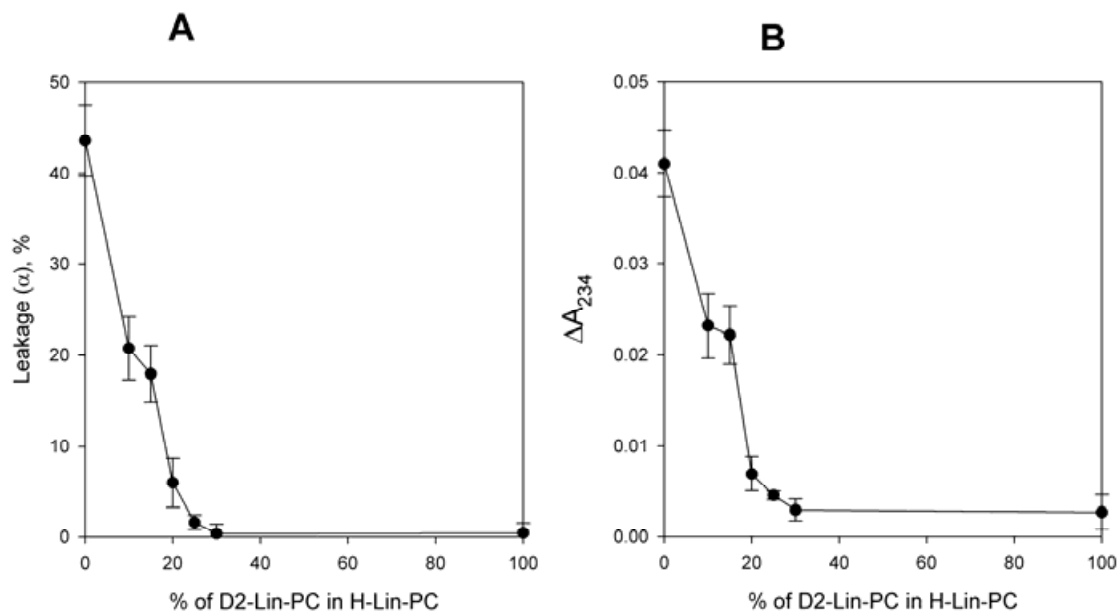


Figure 3. Leakage of SRB (A) and accumulation of diene conjugates (B) in liposomes having various contents of D2-Lin-PC lipid in H-Lin-PC matrix after 10-min incubation with FeSO_4 (5 μM) and ascorbate (100 μM). Experimental conditions as in the legend to Figure 2. The data points represented Mean \pm S.D.

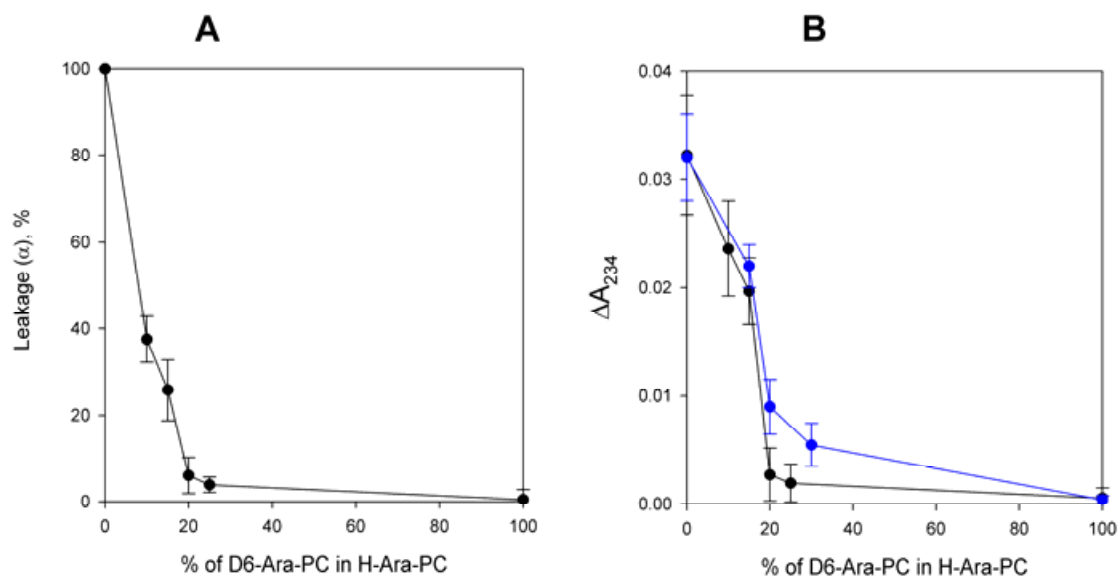


Figure 4. Leakage of SRB (A) and accumulation of diene conjugates (B) in liposomes having different % of D6-Ara-PC lipid in H-Ara-PC matrix (black line) or D2-Lin-PC in the H-Ara-PC matrix (blue line) after 10 min incubation with FeSO_4 (5 μM) and ascorbate (100 μM). Experimental conditions as in the legend to Figure 2. The data points represented Mean \pm S.D.

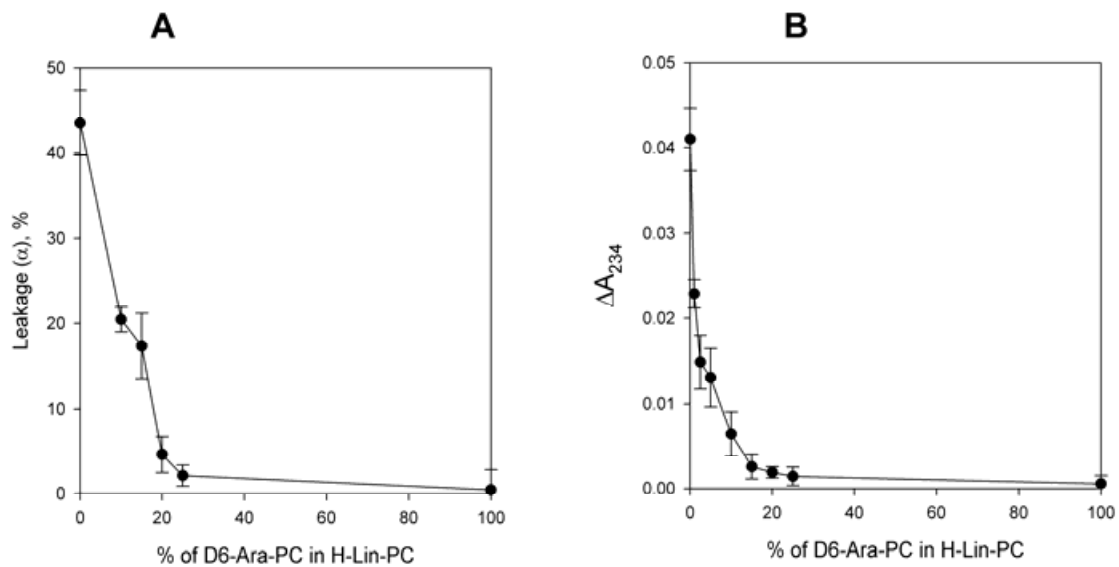


Figure 5. Leakage of SRB (A) and accumulation of diene conjugates (B) in liposomes having various contents of D6-Ara-PC lipid in H-Lin-PC matrix after 10 min incubation with FeSO_4 (5 μM) and ascorbate (100 μM). Experimental conditions as in the legend to Figure 2. The data points represented Mean \pm S.D.

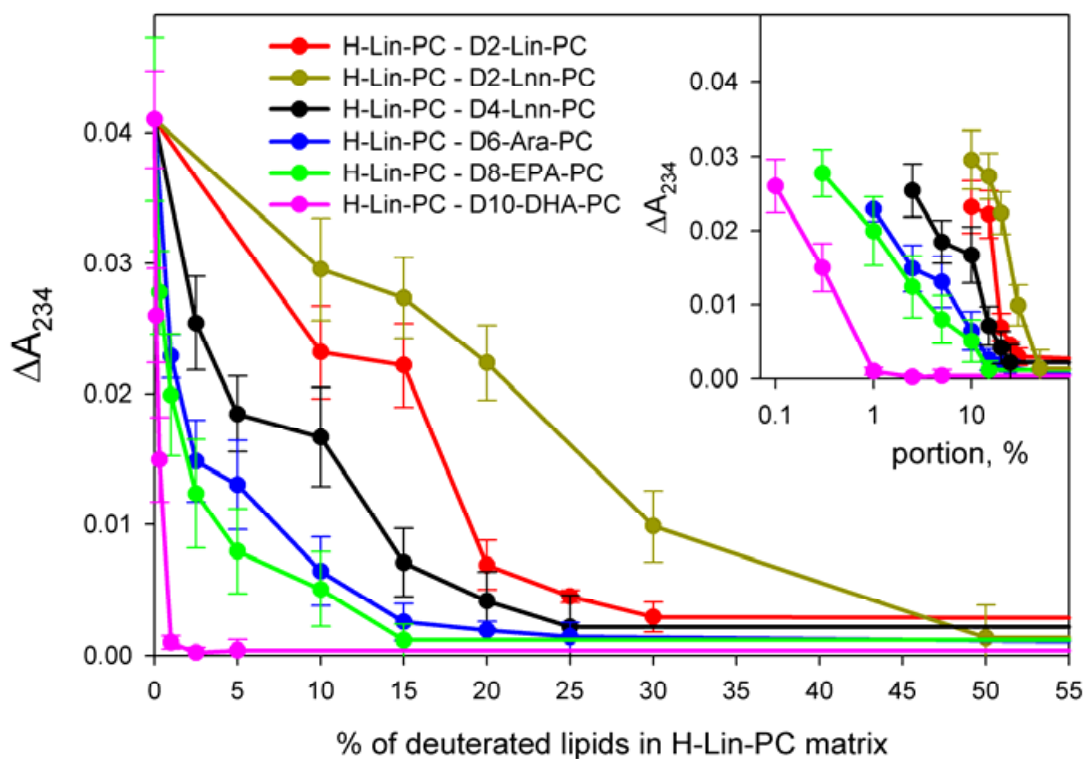


Figure 6. Accumulation of diene conjugates in liposomes having various contents of D10-DHA-PC (pink curve), D8-EPA-PC (green curve), D6-Ara-PC (blue curve), D4-Lnn-PC (black curve), D2-Lnn-PC (beige curve) and D2-Lin-PC (red curve) lipid in undeuterated Lin-PC matrix after 10-min incubation with FeSO_4 ($5 \mu\text{M}$) and ascorbate ($100 \mu\text{M}$). Inset: the same plot in semilogarithmic coordinates. Experimental conditions as in the legend to Figure 2. The data points represented $\text{Mean} \pm \text{S.D.}$

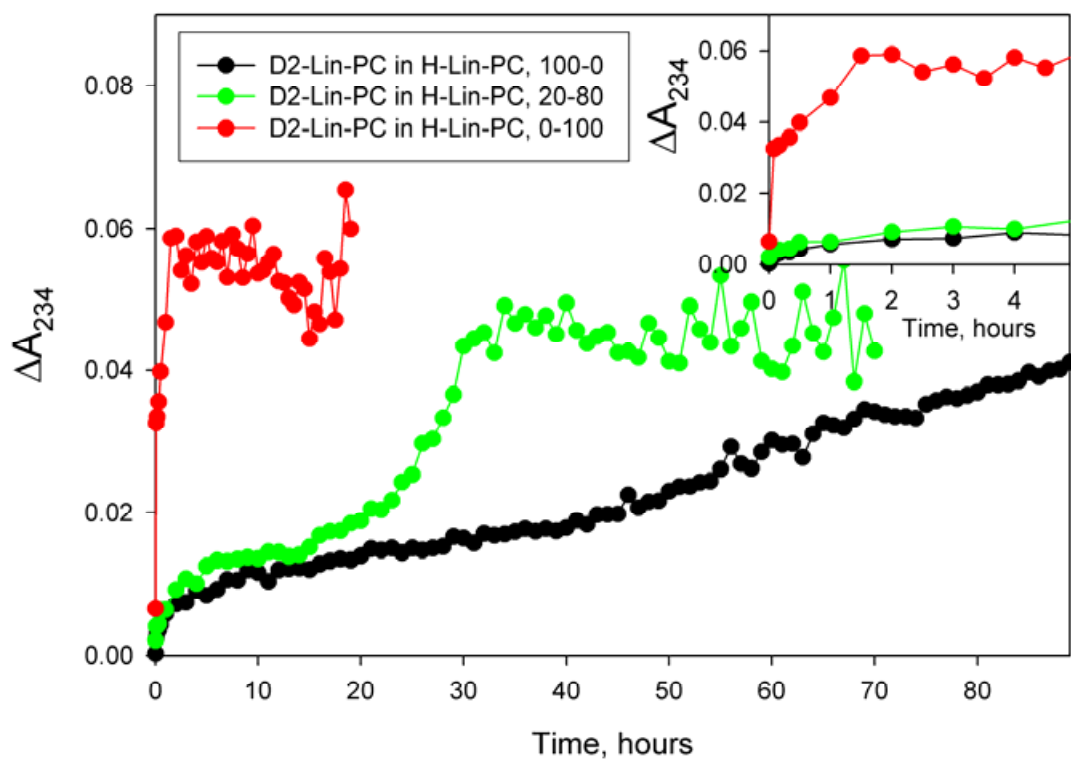


Figure 7. Typical kinetics of accumulation of diene conjugates in 100 % D2-Lin-PC (black curve), 100 % H-Lin-PC (red curve), or a mixture of 20 % D2-Lin-PC and 80 % H-Lin-PC (green curve). The experimental conditions were as in the legend to Fig.2.

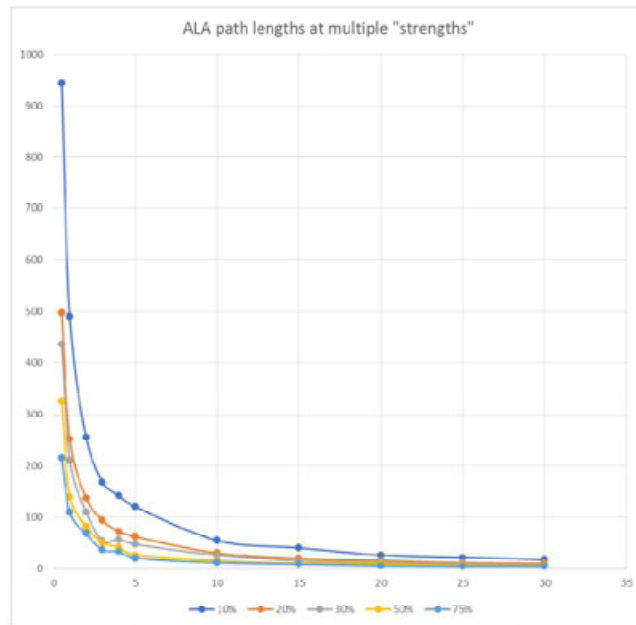


Figure 8. Monte-Carlo simulation of the threshold effect. The vertical axis is the "path length", e.g. the number of H-PUFAs "damaged" before the chain is ultimately terminated. The horizontal axis is the % of the total 2D cells that are D-PUFAs, while the rest are H-PUFAs. Model results are shown for five different "strengths."